SMITHSONIAN INSTITUTION
ASTROPHYSICAL OBSERVATORY

Research in Space Science

SPECIAL REPORT

Number 221

RADAR DOPPLER SPECTROSCOPY OF MARS
I. ELEVATION DIFFERENCES BETWEEN BRIGHT AND DARK AREAS

Carl Sagan, James B. Pollack, and Richard M. Goldstein

GPO PRICE $ _____

CFSTI PRICE(S) $ _____ September 6, 1966

Hard copy (HC) 3.00

Microfiche (MF) .75

ff 653 July 65

CAMBRIDGE, MASSACHUSETTS 02138

SAO Special Report No. 221

RADAR DOPPLER SPECTROSCOPY OF MARS

I. ELEVATION DIFFERENCES BETWEEN BRIGHT AND DARK AREAS

Carl Sagan, James B. Pollack, and Richard M. Goldstein

Smithsonian Institution
Astrophysical Observatory
Cambridge, Massachusetts 02138

6-66-1

TABLE OF CONTENTS

LIST OF TABLES

LIST OF ILLUSTRATIONS

ABSTRACT

12271

This paper is an analysis of radar observations of Mars, particularly at 12.5-cm wavelength, performed at the Goldstone facility of the Jet Propulsion Laboratory, during the 1965 opposition. Then the entire range of Martian longitudes at North latitude 21.6° was observed with an effective topographical resolution in the quasi-specular component of some 6 planetocentric degrees. Both for the 1963 and for the 1965 oppositions a very striking correlation is noted between high reflectivity at radar frequencies, and dark areas at optical frequencies. The correlation applies to the central longitude of the Martian features, to the extent of the features, and to their relative reflectivity rankings at the two frequencies. Despite these correlations, there are occasional displacements between the reflectivity maxima and the centers of dark areas of the order of 10°. This is greater than the expected errors in Martian cartography and in the location of the radar subterrestrial point on Mars. For example, Syrtis Major appears as a radar reflectivity relative minimum, while the 10° longitude strips east and west of Syrtis Major appear as relative maxima. Such observations can be explained — while retaining the hypothesis that the Martian dark areas are intrinsically more reflective at microwave frequencies — if the dark areas have slopes of several degrees. On this basis alone the dark areas might be either elevations or depressions. Conditions on slopes can also be set for those cases in which strong radar reflection comes from a bright area adjacent to a dark area. In this case, a dark area must have an appropriate two-dimensional alignment (in the plane of the sky) with respect to the radar station. From the fact that only the near sides of elevations, but the far sides of depressions, are suitably oriented for specular backscattering, the comparative alignments of near and far sides make it unlikely that dark areas are depressions, a conclusion also supported by other radar

Author

evidence. The hypothesis that the dark areas are elevations is systematically examined in the 36 Doppler spectrograms of the 1965 opposition, and is found to be consistent with these data. The radar data suggest that the dark areas examined in the 1965 opposition were generally not truncated, but rather sloped gently downward from the center of the dark area scanned. From this fact elevations can be deduced from slopes. It is found that some regions that characteristically undergo marked secular changes have very shallow slopes (1 - 2°) and elevations ~6 km; classical canals have steeper slopes (> 4°) but elevations of the same order; and large dark areas such as Syrtis Major and Moeris Lacus may have elevations between 10 and 20 km. These elevations and slopes are inconsistent neither with optical searches for elevations at the limb, nor with the yield and tensile strengths of ordinary solids under the reduced gravitational acceleration of Mars. The general picture of Mars that emerges is similar to that expected for the Earth, were the oceans removed, the effects of water erosion eliminated, and the relief enhanced by the ratio of the gravitational accelerations on the two planets. The dark areas are similar to continental blocks and the bright areas to dry ocean basins. This conclusion bears adversely on those theories of continental origins that depend on the existence of a liquid planetary core.

RADAR DOPPLER SPECTROSCOPY OF MARS
I. ELEVATION DIFFERENCES BETWEEN BRIGHT AND DARK AREAS[1]

Carl Sagan,[2] James B. Pollack,[3] and Richard M. Goldstein[4]

1. INTRODUCTION

Radar observations of Mars have now been performed by three groups — by Goldstein and Gilmore in 1963 and by Goldstein in 1965, at a wavelength of 12.5 cm, with the Goldstone facility of the Jet Propulsion Laboratory; by Kotelnikov et al. in 1963, at a wavelength of 43 cm, with an unidentified radar facility in the Soviet Union; and by Pettengill and Dyce in 1965, at a wavelength of 70 cm, with the Arecibo Ionospheric Observatory of Cornell University. For all these measurements, signals were returned primarily quasi-specularly from the vicinity of the subterrestrial point on Mars; thus, the radar observations have topographical resolution. Further, reflectivity variations were noted in all measurements as Mars rotated beneath the subterrestrial point. These circumstances permit correlations to be drawn between features observed at radar frequencies and those observed at optical frequencies; such correlations cannot be drawn for Venus.

---

[1] This work was supported in part by Grant no. NGR 09-015-023 from the National Aeronautics and Space Administration; and in part by Contract no. NAS 7-100 from the National Aeronautics and Space Administration for that portion carried out at the Jet Propulsion Laboratory, California Institute of Technology, Pasadena, California.

[2] Harvard University and Smithsonian Astrophysical Observatory.

[3] Smithsonian Astrophysical Observatory and Harvard College Observatory.

[4] Jet Propulsion Laboratory, California Institute of Technology.

Goldstein and Gilmore (1963) noted an apparent correlation between a radar-reflection maximum and Syrtis Major, one of the darkest Martian features. Correlations of radar maxima with other dark areas in the 1963 results were reported by Sagan and Pollack (1965) and are further detailed below. However, Dyce (1965) and Goldstein (1965) have called attention to the puzzling facts that radar-reflectivity maxima and optical dark areas do not seem quite correlated in the 1965 data; in fact, in these observations Syrtis Major corresponds to a radar-reflectivity minimum.

The connection between optical and radar observations is explored in detail in the present paper. It will be our contention that the correlation between Martian dark areas and radar-reflectivity maxima is real, and that the apparent correlation anomalies provide evidence for systematic elevation differences between the bright and dark areas of Mars.

2. TOPOGRAPHICAL RESOLUTION

We will begin by estimating the topographical resolution, on Mars, of all sets of radar measurements. Each observer obtained a frequency spectrogram of Mars in which the returned power is examined as a function of the frequency f. Because of the rotation of Mars about its axis, each region of the Martian surface has a characteristic radial velocity along the line of sight to Earth. In particular, power at a given frequency will be returned from a strip on the projected disk of Mars — the projection is normal to the line of sight — which is at a constant perpendicular distance from the projected rotation axis. These strips also approximate strips of constant longitude for a fairly level surface. The central frequency f_c will correspond to the longitude of the subterrestrial point. Surface areas of larger longitude (in the usual convention) will be shifted by the Doppler effect to higher frequencies; areas of smaller longitude to lower frequencies. At the high-longitude equatorial limb the frequency is $f_c + f_0$, while at the low-longitude limb it is $f_c - f_0$. The frequency f_0 is related to the period of rotation P_{σ}, the planetary radius R_{σ}, and the angle χ between the line of sight and the axis of rotation, by the normal expression for the Doppler shift from a moving reflector,

$$f_0 = \Delta f_c = 2 f_c \frac{v}{c} = 2\left[(2\pi/P_{\sigma})\, R_{\sigma} \sin\chi\, (f_c/c)\right] \quad . \qquad (1)$$

Here v is the radial velocity and c the velocity of light.

At a wavelength of 12.5 cm, equation (1) reduces to $f_0/\sin\chi = 3830$ cps. But $\chi = 90° - |D_E|$, where D_E is the planetocentric declination

of the Earth, a quantity tabulated in The American Ephemeris and Nautical Almanac; it is also equal, in absolute value, to the planetocentric latitude of the subterrestrial point. In Table 1 we list the latitudes, in the Northern Hemisphere of Mars, of the subterrestrial point for the 1963 and 1965 oppositions, and derive f_0. The ± values in the D_E column indicate the variation of D_E over the observation period.

Table 1. Planetocentric declination of the Earth, and differential Doppler frequency of the limb for the radar observations

Year	Observer	Wavelength	D_E	f_0
1963	Goldstein and Gilmore (1963)	12.5 cm	+13.8° ± 1.3°	3720 cps
	Kotelnikov et al. (1963)	43	+13.8° ± 1.3°	1080
1965	Goldstein (1963)	12.5	+21.6° ± 0.2°	3560
	Pettengill (1965) and Dyce (1965)	70	+21.6° ± 0.2°	635

The Doppler spectrograms obtained by the observers revealed, analogous to spectra of Venus and the Moon, two components to the reflected power: a quasi-specular component, sharply peaked about f_c; and a more shallow, diffuse component falling off slowly with increasing $|f - f_c|$. The quasi-specular component arises from regions near the subterrestrial point, while the diffuse component arises from regions distributed over the entire planetary disk. We shall use the quasi-specular component to obtain topographical resolution.

Goldstein's (1965) average spectrogram for 1965 (his Figure 9) shows that practically all of the power in the quasi-specular component lies within 370 cps of f_c; a significant fraction lies within 200 cps of f_c.

A frequency displacement of $|f - f_c|$ at equatorial latitudes is related to a displacement in longitude $\Delta\phi$ from the longitude of the subterrestrial point by

$$\frac{|f - f_e|}{f_0} = \sin \Delta\phi = \Delta\phi \quad , \tag{2}$$

where the last equality holds for $\Delta\phi \ll 1$ radian. This approximation introduces errors smaller than those set by the accuracy of the observations themselves in all applications below. Thus, the half-width of the quasi-specular component of these observations corresponds to $\Delta\phi = 6°$. Only longitude strips within 6° of the subterrestrial point (if level) will, on the average, make significant contributions to the quasi-specular component. It is, therefore, reasonable to postulate that only latitudes within 6° of the latitude, D_E, of the subterrestrial point will contribute to the quasi-specular component. Since D_E changes only slightly during the period of observation (cf. Table 1), $\Delta\phi$ also defines the topographical resolution in latitude for points not greatly distant from the equator. The changing longitude of the subterrestrial point then permits us to examine the quasi-specular properties of regions situated in a belt bounded by latitudes $D_E + \Delta\phi$ and $D_E - \Delta\phi$. The length of this belt is defined by the excursion in longitude of the subterrestrial point during the observation period. For all observers save Kotelnikov et al. (1963), the excursion was a full 360° of longitude, and the belt encompassed the planet. The observations of Kotelnikov et al. (1963) were restricted to $310° \leq \phi \leq 360°$ and $0° \leq \phi \leq 140°$.

The belts for 1963 and 1965 are shown, respectively, in Figures 1 and 2, superposed on a map of Mars. The map was prepared by the Space and Information Systems Division of North American Aviation, under the supervision of Dr. A. Dollfus of the Meudon Observatory.

Figure 1. The 1963 radar swath superposed on Dollfus' Martian cartography. (Map prepared by the Space and Information Systems Division, North American Aviation.) The equator and zero meridian of longitude are shown. The middle of the three parallel lines is centered at 13.°8 North latitude, and is bounded by two lines representing the ground resolution of the quasi-specular component of the radar reflectivity. The dark rectangles represent regions of high total radar power reflectivity, and the circles represent regions of relative radar reflectivity maxima. Relevant features coded by number and by letter are as follows:

(1) Mare Acidalium
(3) Aeria
(5) Aethiopis
(6) Amazonis
(7) Amenthes
(9) Arabia
(14) Aurorae Sinus
(24) Ceraunius
(25) Cerberus
(29) Chryse
(39) Deuteronilus
(44) Elysium
(47) Eunostos
(59) Isidis Regio
(60) Ismenius Lacus
(65) Libya
(66) Lunae Palus
(70) Meridianii Sinus
(71) Moab
(72) Moeris Lacus
(75) Nepenthes
(77) Niliacus Lacus
(78) Nilokeras
(80) Nix Olympica
(109) Syrtis Major
(113) Thoth
(116) Thymiamata
(118) Tractus Albus
(120) Trivium Charontis
(126) Xanthe

(A) The recent extension of Nodus Laocoöntis begins just west of this position (cf. Figure 4).
(B) Old position of Nodus Laocoöntis
(D) Astaboras
(E) Eastern Inlet, Dawes' Forked Bay
(F) Western Inlet, Dawes' Forked Bay
(G) Malas Lacus
(H) Mareotis Lacus
(K) Tantalus
(L) Cyane Fons
(P) Titanum Fons

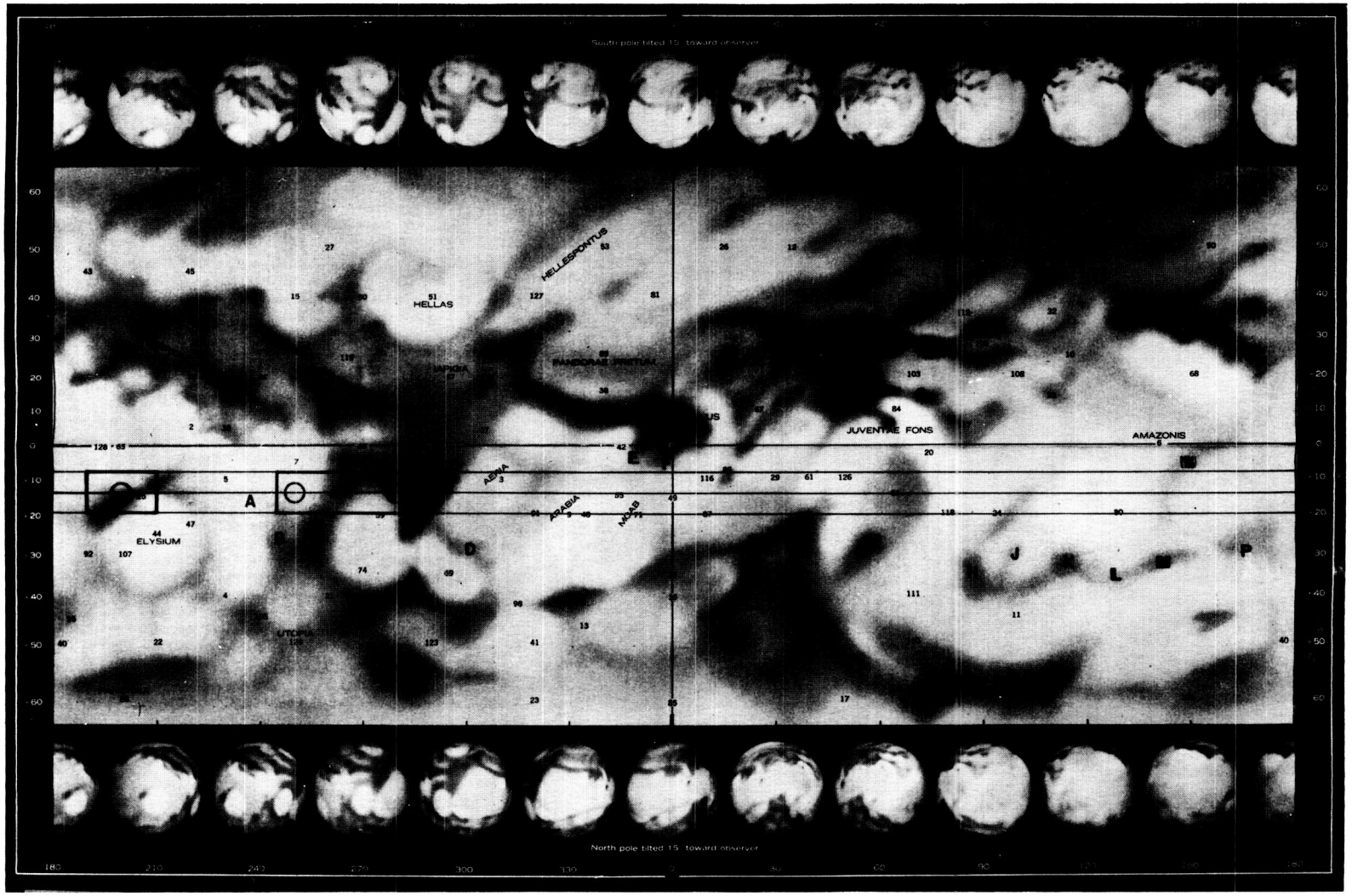
South pole tilted 15° toward observer
HELLESPONTUS
HELLAS
JUVENTAE FONS
AMAZONIS
ELYSIUM
ARABIA
MARE ERYTHRAEUM
UTOPIA
North pole tilted 15° toward observer

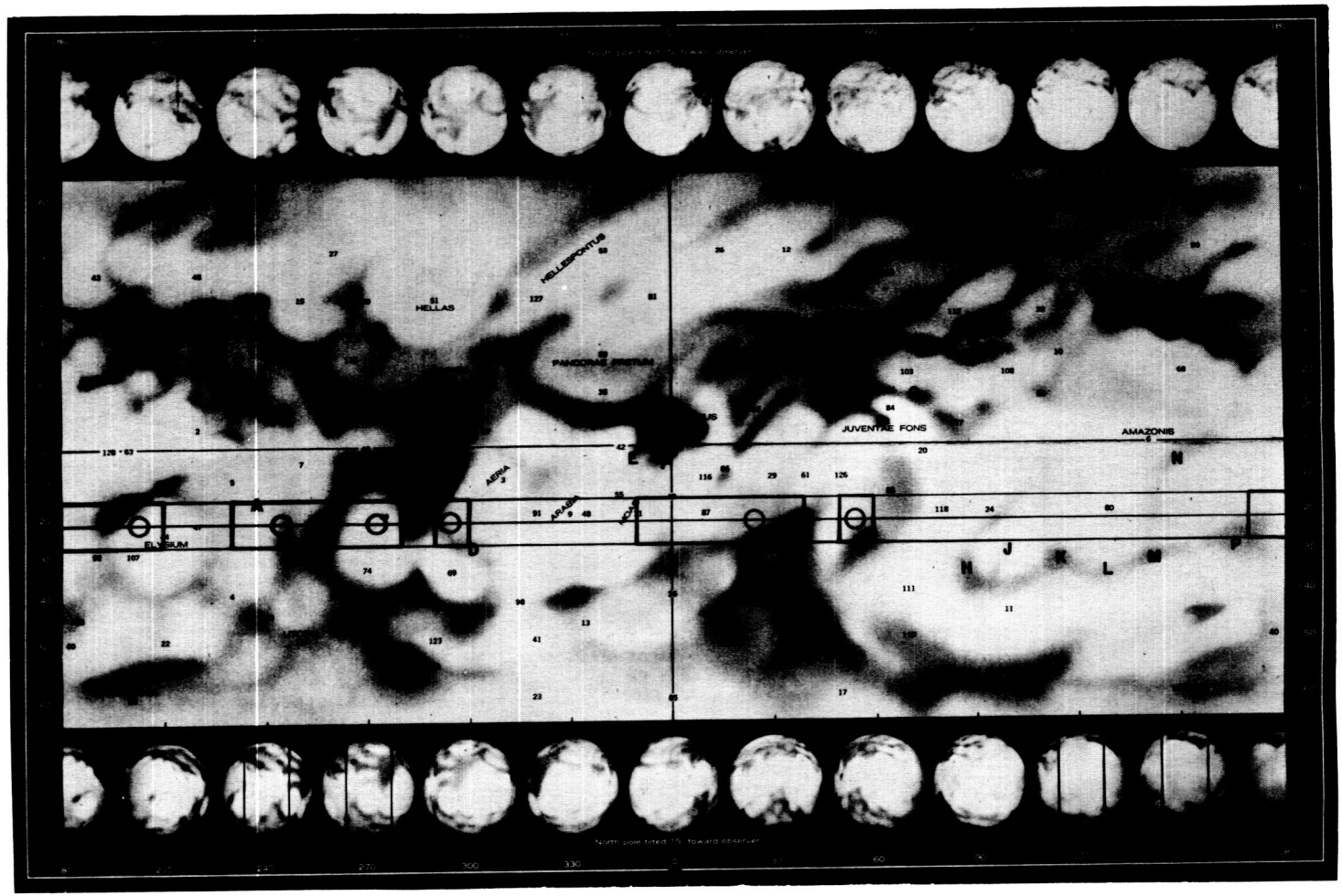

Figure 2. The 1965 radar swath superposed on Dollfus' Martian cartography (map prepared by the Space and Information Systems Division, North American Aviation). The equator and zero meridian of longitude are shown. The middle of the three parallel lines is centered at 21°.6 North latitude and is bounded by two lines representing the ground resolution of the quasi-specular component of the radar reflectivity. The dark rectangles represent regions of high total radar power reflectivity, and the circles represent regions of relative radar reflectivity maxima. The feature code is the same as in Figure 1.

It is in close agreement with the International Astronomical Union Mars cartography [see, e.g., Dollfus (1961).] The positions of optical features on these maps have an uncertainty of plus or minus a few degrees for the latitudes of interest in the present paper. The resolution in longitude is given either by the frequency bandpass $\pm |f - f_c|$ of the quasi-specular component, or by the range of subterrestrial point longitudes over which integration is performed, which ever is the larger. Table 2 displays the bandpasses of interest — either as set by the observers themselves or by our reduction of the data — and the resulting longitude resolution $\Delta\phi$.

Table 2. Bandpass of quasi-specular component and effective longitude resolution.

Facility	Year	$\lvert f - f_c \rvert$	$\Delta\phi$
Goldstone	1963	200 cps	± 4°
U.S.S.R.	1963	2 cps	± 10°
Goldstone	1965	370 cps	± 6°
Arecibo	1965	Data incompletely reduced, but $\Delta\phi$ comparable to 1965 Goldstone results	

The observations of Kotelnikov et al. (1963) have a very low signal-to-noise ratio, $\simeq 2$. Further, these observations indicate more power within an extremely narrow bandpass of ± 2 cps than other observers report with substantially superior signal-to-noise. For these reasons we will not consider these observations further. The Arecibo observations are still in the process of reduction (Dyce, 1966), and only the frequency-integrated power is available at present (Dyce, 1965; see also Pettengill, 1965). We will use these measurements as a check against the higher frequency 1963 and 1965 Goldstone observations, to be considered in detail. The 1963 Goldstone observations are reduced

as a plot of power (within a bandpass of ± 200 cps) vs. longitude. For the 1965 observations, we presently display and analyze Doppler power spectrograms for 36 longitude strips, each 10° in width, the set comprising the entire range of longitudes.

3. CORRELATION OF RADAR REFLECTIVITIES WITH OPTICAL DARK AREAS

We now attempt to correlate Martian surface features observed at optical frequencies with the reflectivities of the quasi-specular components of the returned radar signals. The 1963 Goldstone observations are considered to have an effective bandpass of ± 200 cps. For the 1965 observations, with two choices of effective bandpass — ± 200 cps and ± 370 cps — reflectivities were obtained by planimetry of the spectrograms. The resulting longitude plot is given in histogram form in Figure 3 for the bandpasses 1480-2220 cps and 1620-2080 cps. We see that the general character of the longitude dependence of quasi-specular reflectivity does not depend sensitively on the bandpass chosen.

Figures 1 and 2 show that the radar excursions of 1963 and 1965 primarily traversed Martian bright areas: Elysium, Aethiopis (numbered 5 on these maps), Isidis Regio (59), Aeria, Arabia, Moab (also called Eden), Thymiamata (116), Chryse (29), Xanthe (126), Tractus Albus (118), Nix Olympica (80), and Amazonis. It has been suggested that Nix Olympica is a high plateau, because white clouds are observed to occur preferentially in its vicinity. The 1963 radar swath encountered two major dark areas, the Cerberus — Trivium Charontis complex, and the Nepenthes — Moeris Lacus — Syrtis Major complex. The 1965 swath encountered these same dark areas — although at somewhat more northerly latitudes — and, in addition, passed through the Nodus Laocoöntis — Nepenthes complex, the Deuteronilus — Niliacus Lacus complex, and Nilokeras. A visual map of a portion of Mars for the 1965 opposition appears as Figure 4. It was produced by J. H. Focas of the Athens and Meudon Observatories and its reproduced through the courtesy of Dr. Focas and Dr. Dollfus. The primary new feature near 20° latitude, which appears in the 1965 map, is the greatly enhanced darkness and extent of the Nodus Laocoöntis area, near 250° longitude.

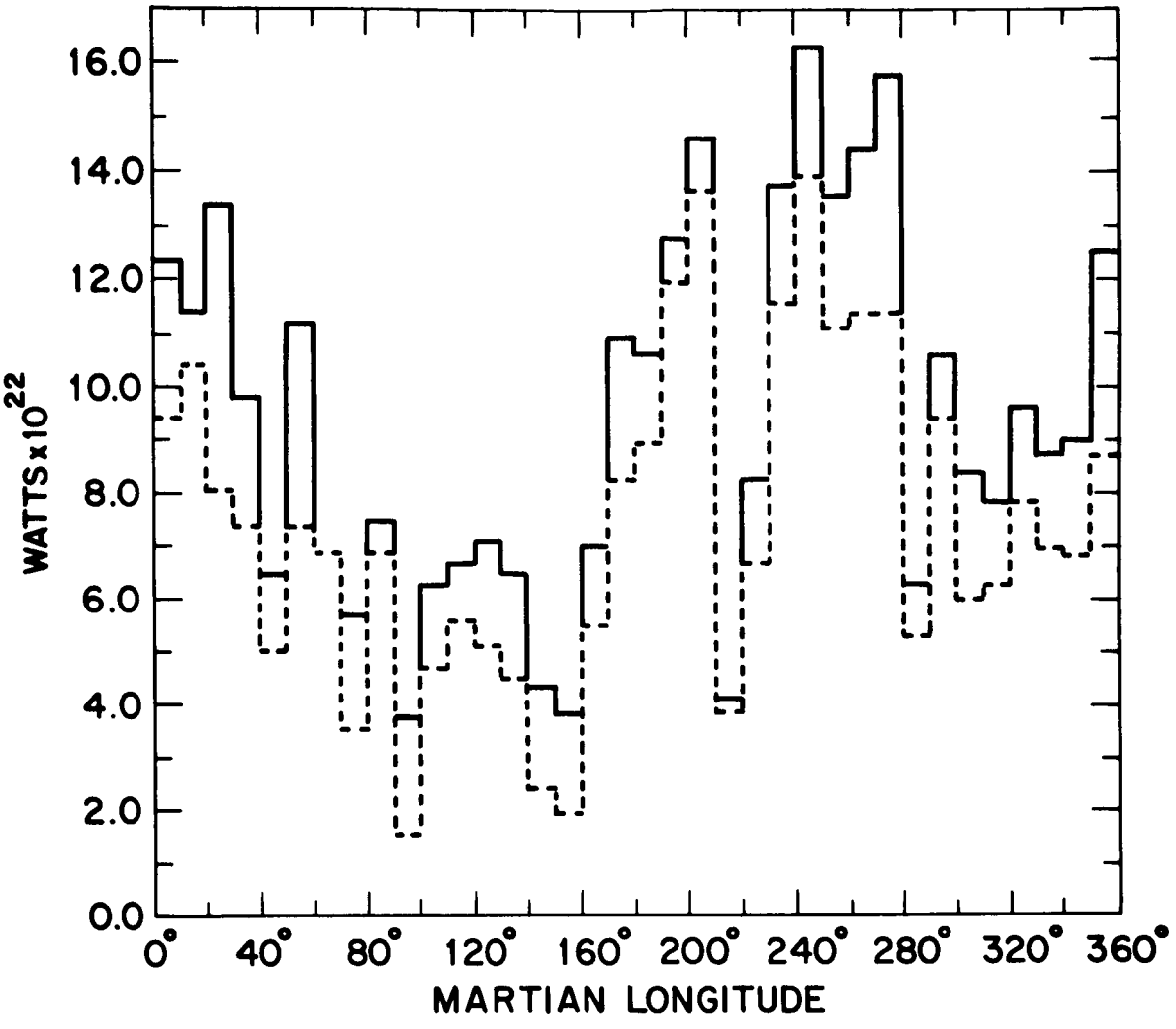

Figure 3. Histograms of total power vs Martian longitude for two choices of bandpass, 1480 - 2220 cps and 1620 - 2080 cps. The figure was derived by planimetry of the 1965 Goldstone radar observations.

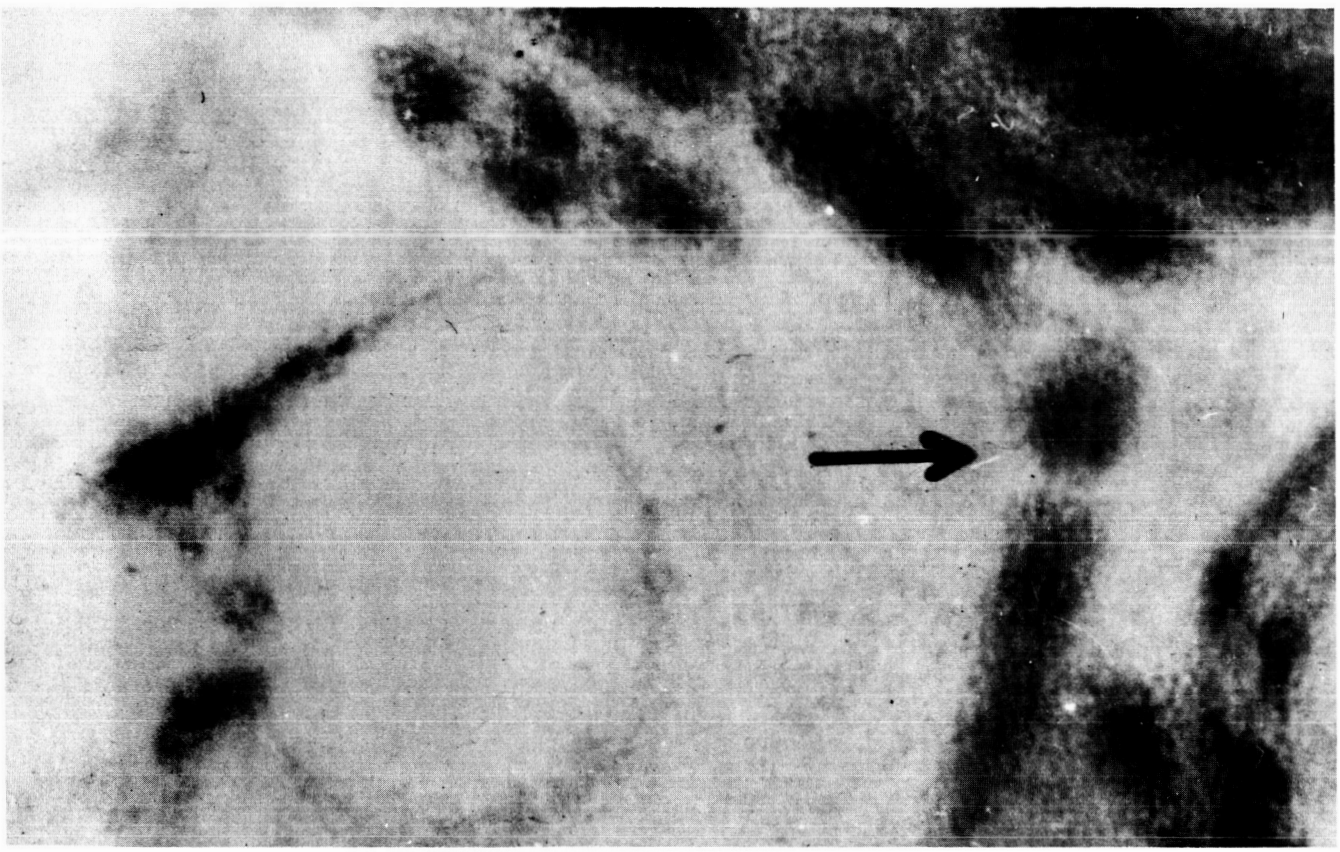

Figure 4. A visual map of Mars during the 1965 opposition, prepared by Dr. J. H. Focas of the Athens and Meudon Observatories. The arrow points to the break in the extension of Nodus Laocoöntis, a feature having undergone a major secular change during the last few years. Courtesy of Dr. Focas and Dr. A. Dollfus.

In Figures 1 and 2, zones of high radar reflectivity are shown as dark rectangles, superposed on the map of Mars. The principal relative maxima in radar reflectivity are shown as circles of radius $\Delta\phi/2$. Locations of reflection maxima can be determined to better than $\pm$ 5° by comparison with adjacent longitude strips. A maximum within $\sim$3° of a neighboring strip will have its position better refined by noting the high total power of the neighboring strip; similarly a maximum more than about 7° from a neighboring strip can have its position refined by noting the low total power of the neighboring strip. Comparison between optical and radar results is also given in Table 3. It is evident that the extent and position of regions of high radar reflectivity bear an almost one-to-one relation with the extent and position of the dark areas traversed by radar in both the 1963 and 1965 oppositions. Moreover, the positions of the relative-reflectivity maxima lie within 10° of longitude of the major dark areas. The optical ranking of dark areas in the last column of Table 3 is based on the visual albedo of the area in question and the extent to which it fills the area resolved by the quasi-specular component of the radar beam. Special attention has been given to the comparitive prominence of the Nodus Laocoöntis region in the 1965 opposition. We see that the optical darkness and radar-reflectivity rankings have a good correlation, the only exception being for the 295° longitude feature in the 1965 observations. The only apparent puzzle (the subject of the next section) is the occasional displacement of radar-reflectivity maxima by $\sim$10° from the nearest dark area. We conclude in this section that the Martian dark areas show a systematically stronger quasi-specular radar reflectivity than the Martian bright areas. An explanation of this difference is offered elsewhere (Sagan and Pollack, 1965; Pollack and Sagan, 1966).

Table 3. Correlation of regions of high quasi-specular radar reflectivity with optical dark areas on Mars.

Observing station and opposition	Bandpass cps	Longitude of reflection maximum	$\frac{R}{R_{max}}$	Reflection ranking	Extent of maximum (in longitude)	Corresponding optical feature	Central longitude of feature	Extent of feature	Darkness ranking
Goldstone Tracking station 1963	400	200 ± 5°	0.70	3	190 - 210°	Cerberus-Trivium Charontis	205°	195 - 210°	4
						Nodus Laocoöntis	250°	245 - 255°	2
		250 ± 5°	0.90	2	245 - 290°	Nepenthes	265°	250 - 260°	3
		280 ± 5°	1.00	1		Moeris Lacus		255 - 270°	3
						Syrtis Major	285°	270 - 295°	1
Goldstone Tracking station 1965	740	25 ± 3°	0.80	4	350 - 40°	Deuteronilus, Niliacus Lacus	35°	360 - 20°	3
								20 - 40°	1
		55 ± 3°	0.70	5	50 - 60°	Nilokeras	55°	50 - 60°	1
									5
		203 ± 3°	0.90	3	170 - 210°	Trivium Charontis	195°	190 - 205°	4
		245 ± 3°	1.00	1	230 - 280°	Nodus Laocoöntis, Nepenthes	247° 260°	245 - 270°	2
		273 ± 3°	0.95	2		Syrtis Major	285°	280 - 295°	1
		295 ± 3°	0.65	6	290 - 300°	Syrtis Major	285°	280 - 295°	1

4. THE EFFECT OF ELEVATION DIFFERENCES

Despite the very good correlation of radar-reflection maxima with the central longitudes of the dark areas, their occasional mutual longitude displacements – characteristically ~10° – remain to be explained. Let us first convince ourselves that the displacements are real. Might the combined errors in knowledge of the central meridian for the radar observations and in photographic cartography amount to net errors of some 10°? From Figures 2 and 4 we see that no displacement can explain the lack of exact coincidence in the radar and optical results. At an average opposition a resolution of 1 sec of arc corresponds to about 8 equational longitude degrees on Mars. However, by observing at favorable oppositions, by superposing photographs, and by higher resolution micrometer and other visual checks, the uncertainties in the configuration and positions of features have been reduced to 2 or 3 degrees at most (Dollfus, 1965). Moreover, the positions of centroids of Martian features are much better known than their shapes, and it is the positions of centroids rather than shapes that are critical in evaluating correlations between radar and optical features. The radar longitudes depend on the position of the zero meridian in Sinus Meridiani. After many decades of precise time observations this is known to a very small fraction of a degree. Because of signal-to-noise limitations, radar reflectivities are known in general only to within 10°-strips of longitude. If, however, a strong return is received from an area near the borders of such a 10°-strip, its presence should also be manifest from the reflectivity of adjacent strips. In this way the positions of strong radar maxima are known to about ± 3°. Thus, errors in position cannot explain displacements of ~ 10°.

In addition, the general location of broad radar-reflection maxima (the rectangles of Figures 1 and 2) cannot be understood merely by association with dark areas; high reflectivities obviously exist in bright areas adjacent to dark areas. The observed radar return may in part come from some effective subsurface reflecting layer significantly beneath the surface optical-reflecting layer (Pollack and Sagan, 1966). Regardless of the nature of this subsurface layer, it clearly can be covered by a visually reflecting layer of surface material transparent to microwaves, and we can picture the Martian dark areas to have a greater extent at microwave than at optical frequencies. While this helps to account for the extent of the high-reflectivity rectangular areas of Figures 1 and 2, it cannot explain, for example, the well-defined radar-reflectivity minimum just at Syrtis Major in both the Goldstone and the Arecibo 1965 data; nor a similar occurrence in the 1963 Goldstone data; nor why the 1965 reflectivity at 30-40° longitude, which is very close to Niliacus Lacus, is less intense than that at 20-30°, which is more distant from this dark area (see Figures 1-3).

These anomalies are readily explicable, however, if we assume systematic elevation differences between the bright and dark areas. For example, assume Syrtis Major is an elevation that slopes gently upward from its periphery toward its center with an average slope of a few degrees. It is then immediately clear that with the subterrestrial point several degrees in longitude away, the slope of Syrtis Major will be such that the receiver on Earth will see a specular reflection; while, when the feature is centered under the subterrestrial point, the slopes will deflect the bulk of the power away from Earth and backscattering will be small. This situation and the analogous one, if Syrtis Major is a depression, are illustrated in Figure 5. We are thus lead to postulate that the Martian dark areas are regions of intrinsically high radar reflectivity, but which have a mean slope that is tilted with respect to their surroundings. Note

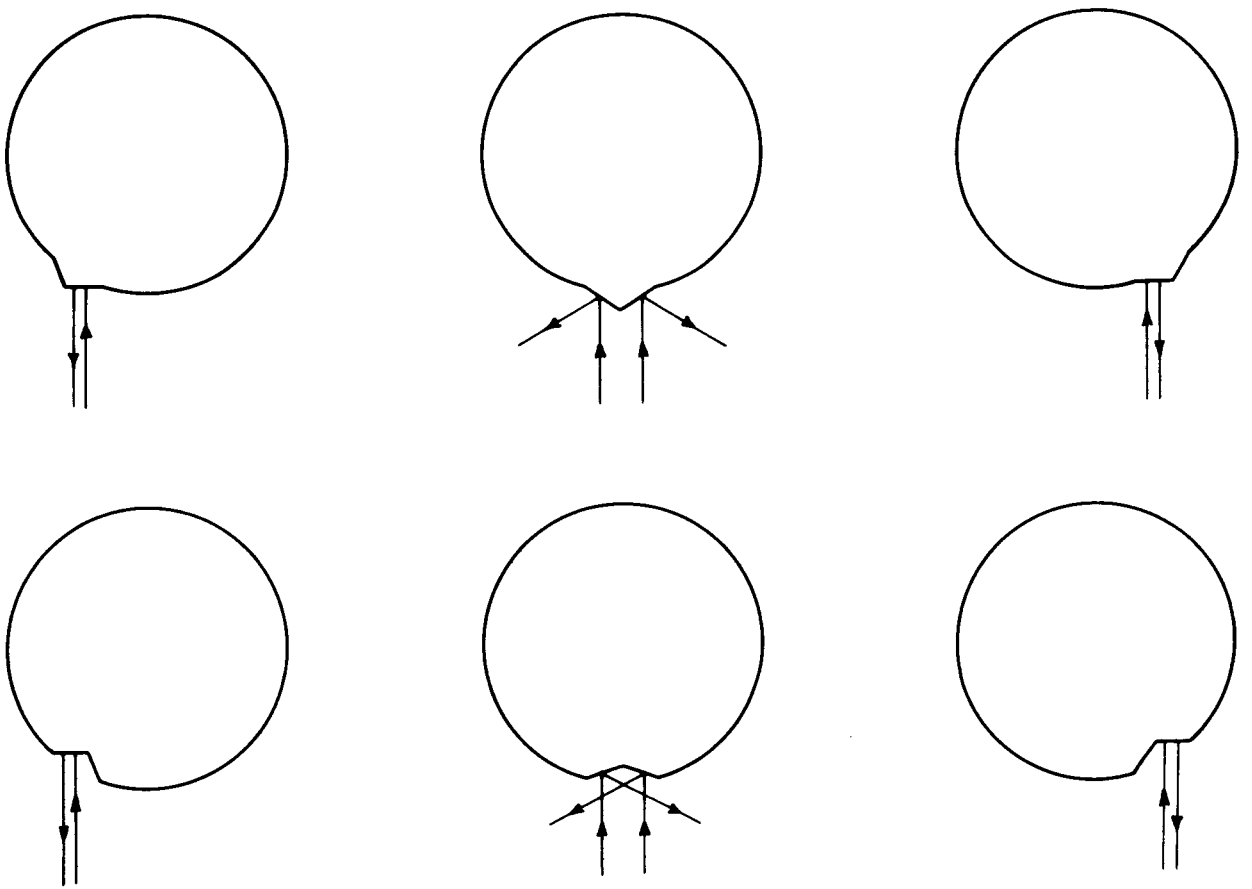

Figure 5. Schematic representation of the effects of Martian elevations and depressions on the radar backscatter. Enhanced reflectivities arise from the near sides of elevations and from the far sides of depressions. When the elevation or depression is under the subterrestrial point (top middle and bottom middle), backscattering in the direction of Earth is small. However, when the feature is displaced from the subterrestrial point by a planetocentric angular distance equal to its mean slope, enhanced specular backscatter occurs.

that we achieve the same effect whether the inclined dark area is to the east or to the west of the subterrestrial point. Because of this symmetry, we can refer directly to Figures 1 and 2, despite the fact that in them the telescopic cardinal point convention is used, inverting east and west, and north and south, as seen by the naked eye.

We now examine the effects of our postulated slopes in more detail. Let $\bar{a}$ be the mean slope on either side of the center of a dark area with respect to the surrounding bright areas, and let $2\Delta a$ be the spread in tilt angles. When $\bar{a} < \Delta a$, many surface facets specularly reflect to Earth and we have the usual case of quasi-specular reflection; maximum power within the quasi-specular component then occurs when the feature is centered at the subterrestrial point. The 1963 maximum in the Cerberus – Trivium Charontis complex (Figure 1) illustrates this case.

However, when $\bar{a} \simeq \Delta a$ the situation greatly changes. Now, when a highly reflective area fills the region about the subterrestrial point, only a small fraction of the area will, in general, contribute to the returned power; the mean slope overwhelms the randomly oriented facets. The 1965 minimum in Syrtis Major (Figure 2) illustrates this case.

We next consider for these two cases the contribution to the radar return when the subterrestrial point is nearby but not within the inclined region. It is our expectation that facets will tend to be oriented in the plane of the general slope, rather than at right angles to it. When $\bar{a} \simeq \Delta a$ few facets will be properly oriented for reflection back to Earth unless the entire dark area is properly aligned in two dimensions in the plane of the sky. When $\Delta a > \bar{a}$ there is a greater probability that facets will, by chance, be oriented for reflection to Earth, but the observed radar return will still be very significantly enhanced if the

entire dark area is properly aligned. In the case of proper alignment the dark area should be distant from the subterrestrial point an angular distance in planetocentric coordinates between $\bar{\alpha} + \Delta\alpha$ and $\bar{\alpha} - \Delta\alpha$. In the case of poor alignment the dark area must be $\pm \Delta\alpha$ from the subterrestrial point for a strong radar return.

Proper alignment in the above sense is equivalent to the following condition: for strong reflection, a line drawn in the plane of the sky from the subterrestrial point to the dark area should coincide with the normal to the border between the dark area and the adjacent bright area. We would not expect $\bar{\alpha}$ or $\Delta\alpha$ to be more than several degrees on Mars, and therefore would not expect dark areas more distant than about 10° to contribute significantly to radar returns when the subterrestrial point is in a bright area. In Figure 6 arrows have been drawn from all dark areas near latitude 21.°6 that seem properly aligned to contribute to radar returns in the 1965 data. Comparison of Figures 6 and 2 shows excellent agreement. The principal radar returns all come from bright-area regions close to properly aligned dark areas. Other features of the reflectivity then also become clear. The alignment of Trivium Charontis is unfavorable for a specular return at 180 - 190°, but very favorable for a specular return at 200 - 210°, an equal distance away. The data (Figure 3) show a pronounced relative maximum at 200 - 210°, and a relative minimum at 180 - 190°.

We must now consider whether the dark areas are elevations or depressions. Totally independent evidence from several directions can be marshalled that strongly indicate the former alternative (Sagan and Pollack, 1966), but we here content ourselves primarily with radar evidence. First, consider the possibility that the bright and dark areas are both broken up into a series of elevations and depressions with flat tops and bottoms. In this case it would be difficult to understand why, e. g., Syrtis Major is a

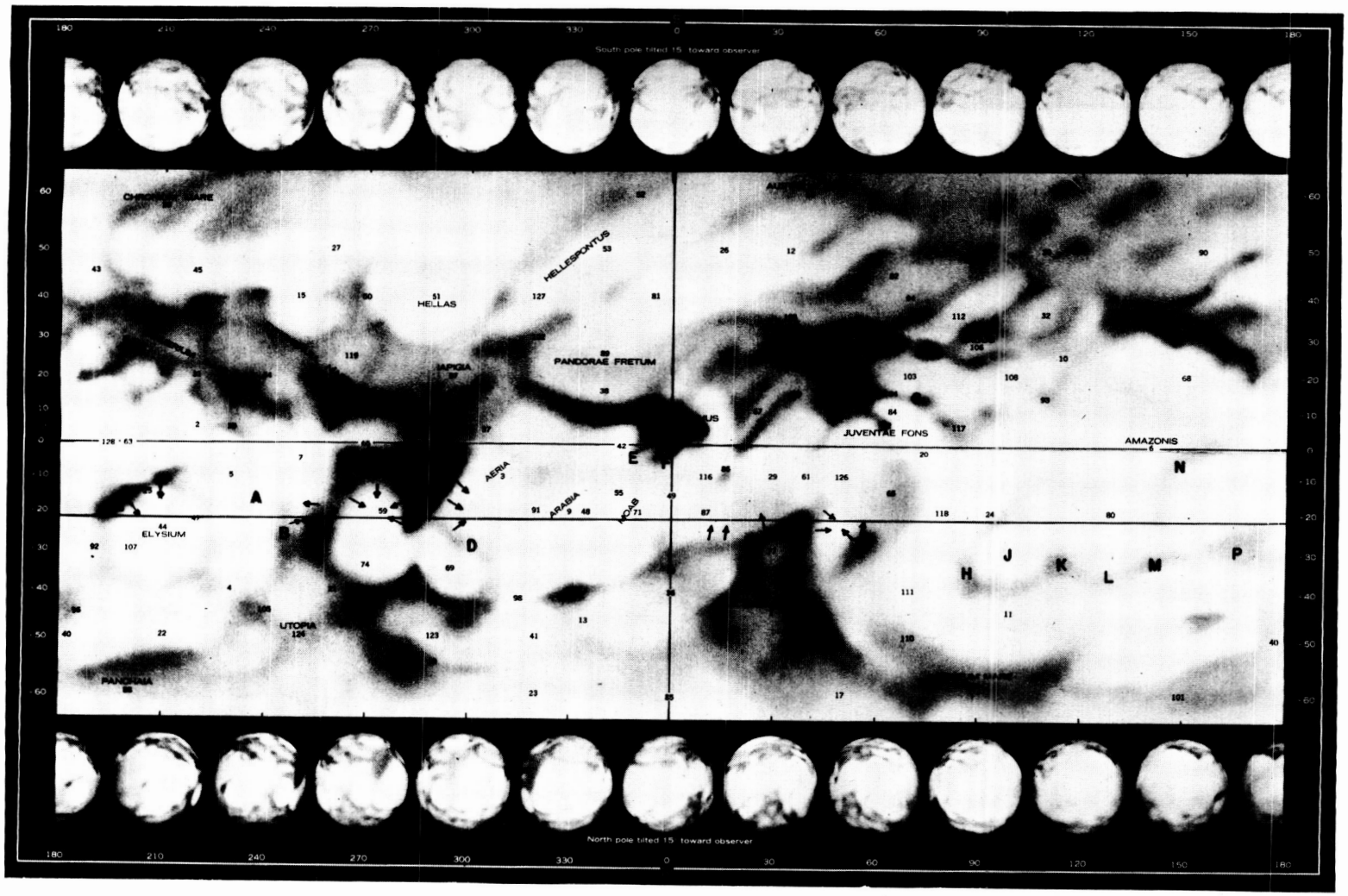

Figure 6. Alignment of dark areas (near the 21°.6 central latitude of the 1965 radar observations) producing expected enhancements of the radar return when the subterrestrial point lies in adjacent bright areas. Cf. Figure 2.

radar-reflectivity relative minimum; the flat regions, should reflect quasi-specularly. We assume, initially, that that the dark areas are either large elevations or large depressions. For reasons of economy of hypothesis, we consider it unlikely that some dark areas are elevations and others depressions. An observational distinction between elevations and depressions is achieved if we know which side of the dark area contributes to the radar-reflection maximum. As illustrated in Figure 5, only the near sides of elevations and the far sides of depressions are suitably oriented for specular backscattering.

Accordingly, we consider the longitude strip 270 - 280° in the 1965 Goldstone data. The subterrestrial point lies in the Isidis Regio desert. The far sides of the adjacent dark areas are sizable distances away (~ 20° planetocentric), and quite steep slopes — very unlikely on so dusty a planet as Mars — are required to understand the high radar reflectivity if the dark areas are lowlands. On the other hand, the near boundaries of Moeris Lacus and Syrtis Major are acceptably close and are properly aligned (cf. Figure 6); the high radar reflectivity can be understood if the dark areas are highlands.

Similarly, a strong and very narrow quasi-specular reflection is observed in the 200 - 210° longitude strip. Here the subterrestrial point is in the Elysium desert, and from the spectrogram (see discussion below) it follows that only longitudes within 1.5° of the subterrestrial point contribute. The 1965 Arecibo total power peaks at 201° longitude. These results can be understood as an effect of the near side of Trivium Charontis when the subterrestrial point is near 200°. But it would be difficult to understand the narrowness of the quasi-specular component and its location about f_c were the far side of Trivium Charontis responsible. Several similar situations will emerge in the detailed spectral analysis below, where confirmatory evidence will be presented. For the moment, we conclude that unless fairly steep slopes exist on Mars, dark areas are highlands.

5. SYSTEMATIC DISCUSSION OF THE SPECTRA

We now proceed to discuss the 1965 Goldstone spectra (see Goldstein, 1965) in detail. Signals were transmitted to Mars for a period of 11 min (the round-trip time of flight), and then received for 11 min. The limb-to-limb Doppler broadening due to the rotation of Mars and allowing for $\sin \chi$ in equation (1) is 7670 cps compared with the instrumental bandpass of 3700 cps; this bandpass, therefore, rejects the small amounts of limb backscatter. The frequency resolution was 84 cps, corresponding, from equation (2), to a longitude difference of about 1°.4.

Each 10°-longitude strip displayed below represents an integration of observations at more circumscribed longitudes within the strip — an integration performed to increase the signal-to-noise ratio. While spectral features should ordinarily refer to the middle of the strip, some may refer to signals returned when the subterrestrial point was near the borders of the strip.

The typical Doppler spectrum will have both a quasi-specular and a diffuse component. A small quasi-specular component may arise even when the subterrestrial point is in a bright area of low intrinsic radar reflectivity. When a strong radar signal is returned from a bright area the quasi-specular component will have contributions both from the bright area itself and from adjacent dark areas with suitable slopes and alignments. The width of the quasi-specular component provides information on the displacement of contributing dark areas; asymmetries in the quasi-specular component may be useful in identifying contributing dark areas. Properly aligned dark areas of suitable slope, which are a fair number of planetocentric degrees from the subterrestrial point, may be detected by high- or low-frequency satellites of the quasi-specular peak.

In the analysis of the spectra below, we have performed eye estimates of what constitutes an acceptable signal-to-noise ratio. We have considered the general noise level, especially at the periphery of the diffuse component; both the sharp central peak (if any) and the centroid of a quasi-specular component; and the general regularity that the quasi-specular component ordinarily lies entirely above the zero signal level, while the diffuse component tends to fade into the noise.

Figures 7-42 are the Doppler radar spectra of the 36 longitude strips — each 10° wide — that comprise the complete swath near latitude 21.°6 observed at Goldstone in 1965. The central frequency is indicated by the vertical line. Because of the sign conventions of our maps, increasing longitude conveniently corresponds to increasing frequency, the conversion being, approximately, 0.1 Kc = 18° of longitude. We now discuss each spectrum, starting at the generally uninteresting longitude strip 320 - 330°. After this discussion, the principal results will be summarized in Table 4.

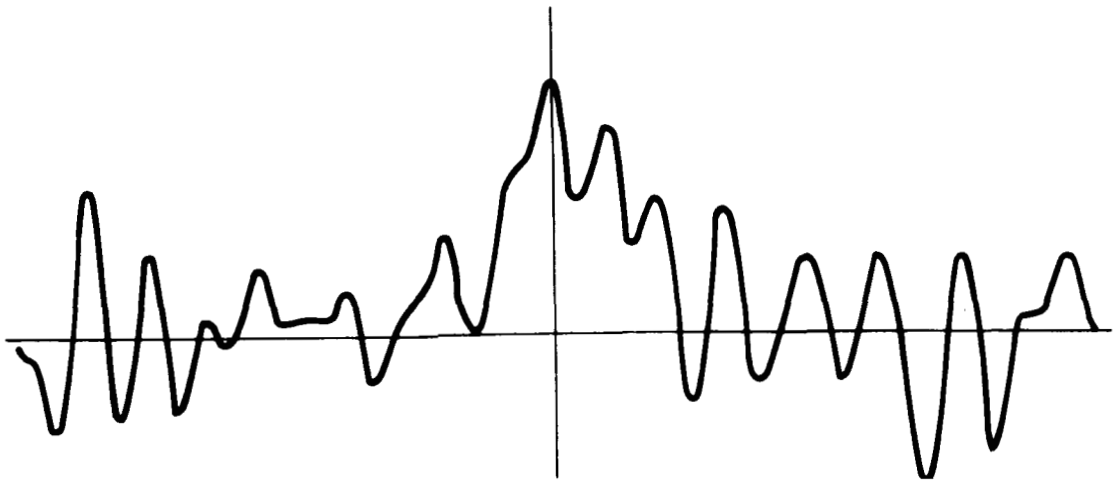

Figure 7. 320 - 330°.

The centroid of the quasi-specular component may possibly be shifted a few degrees to higher longitudes. The southern border of Ismenius Lacus has a suitable longitude and good two-dimensional alignment; but its required slope would have to be steep, ~ 15°, to account for this possibly real asymmetry. The general reflectivity here is due to the bright area, Arabia.

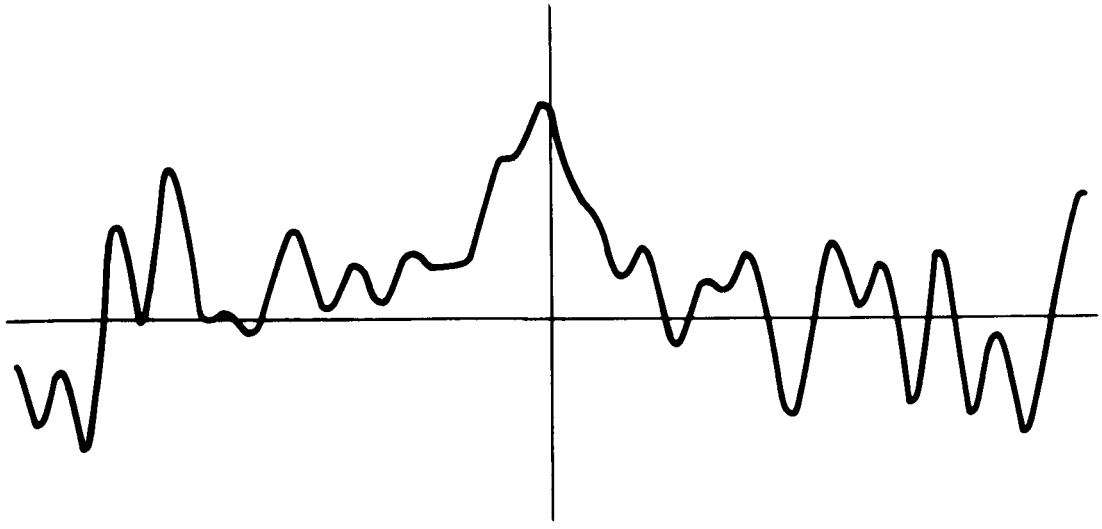

Figure 8. 330 - 340°.

To within the error of measurement, the quasi-specular component is symmetric about the central frequency, and no significant satellite reflection maxima exist. If Ismenius Lacus were contributing to the 320 - 330° spectrum it would contribute symmetrically here. Deuteronilus, invoked in later spectra, is too poorly aligned to contribute here.

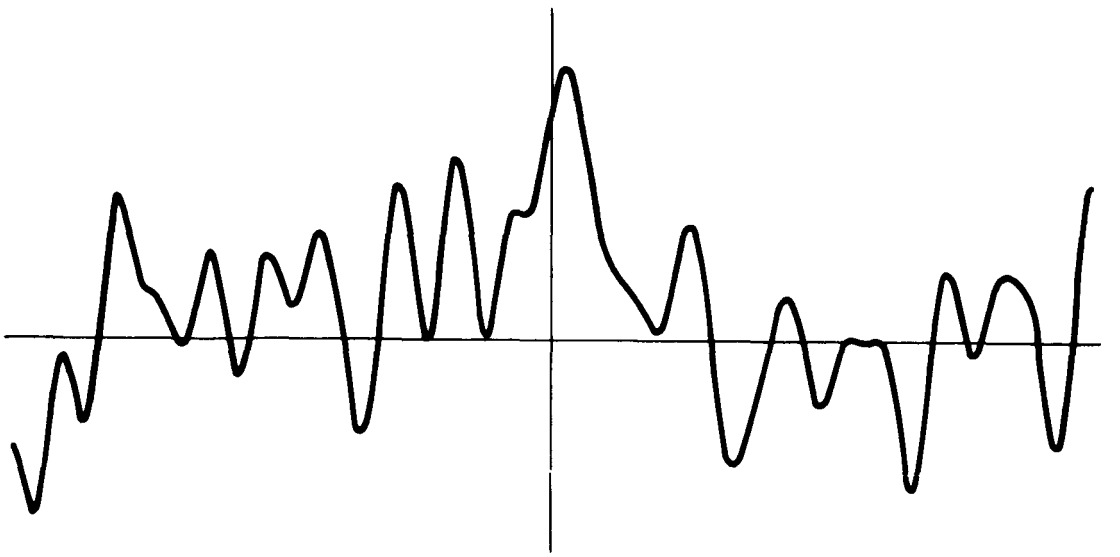

Figure 9. 340 - 350°.

To within the error of measurement on this (noisy) spectrogram, the centroid of the quasi-specular component may be shifted a few degrees to higher longitudes. A segment of Deuteronilus is correctly positioned and aligned; the required slopes are high, however, ~12°.

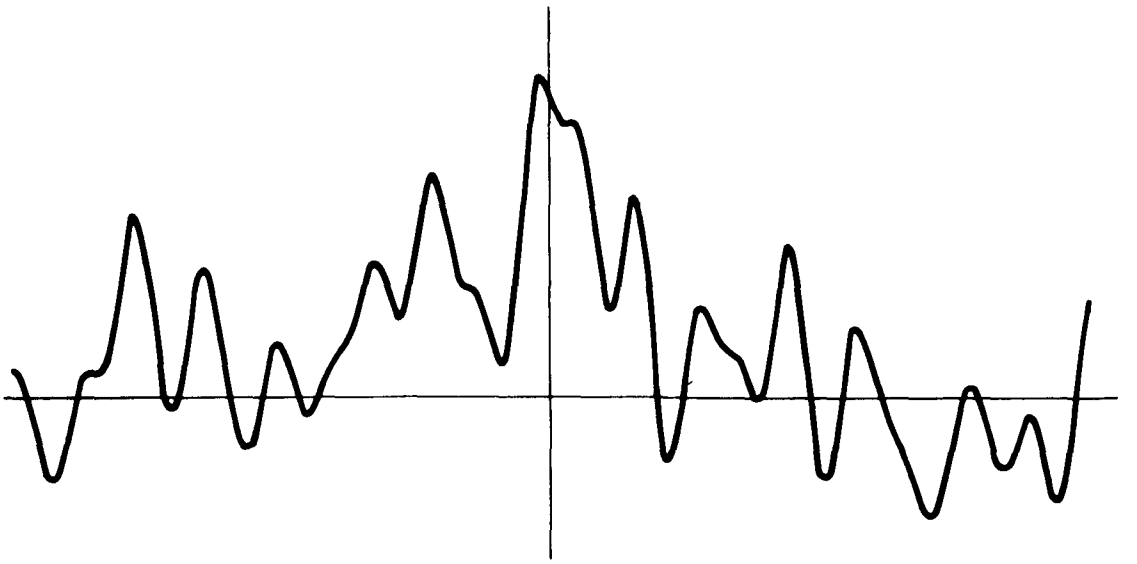

Figure 10. 350 - 360°.

This longitude range begins a region of high radar reflectivity extending to 30 - 40° (see Figure 2). There is a distinct high-frequency asymmetry to the quasi-specular component, which we attribute to a segment of Deuteronilus, which has the appropriate longitude, good alignment, and is now relatively nearby.

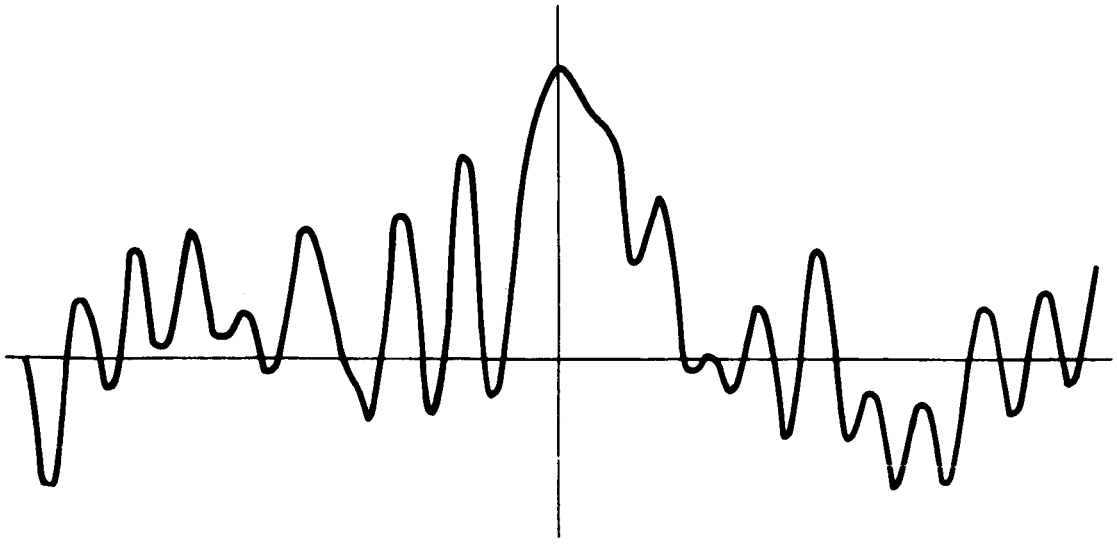

Figure 11. 0 - 10°.

The quasi-specular component has a high-frequency asymmetry due again to Deuteronilus, now about 6° away, but with poorer alignment than in preceding spectra.

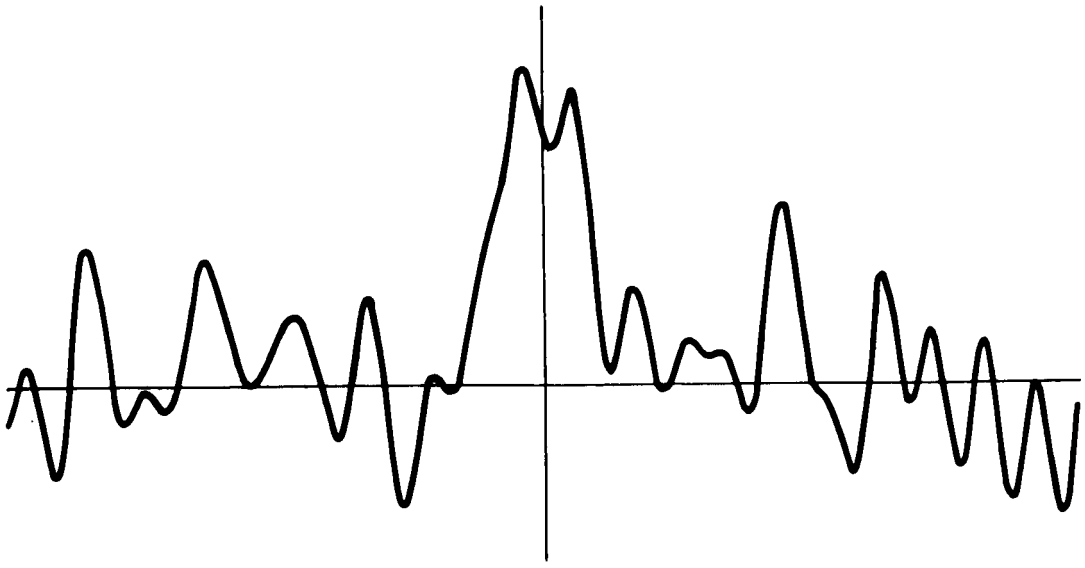

Figure 12. 10 - 20°.

The marked quasi-specular component is entirely symmetrical about the subterrestrial point. This is understandable, because the subterrestrial point now lies symmetrically south of Deuteronilus, which has now turned in an east-west orientation. Deuteronilus is aligned well, and is only a few degrees away. There are no segments of Deuteronilus properly aligned to give asymmetric components at this longitude.

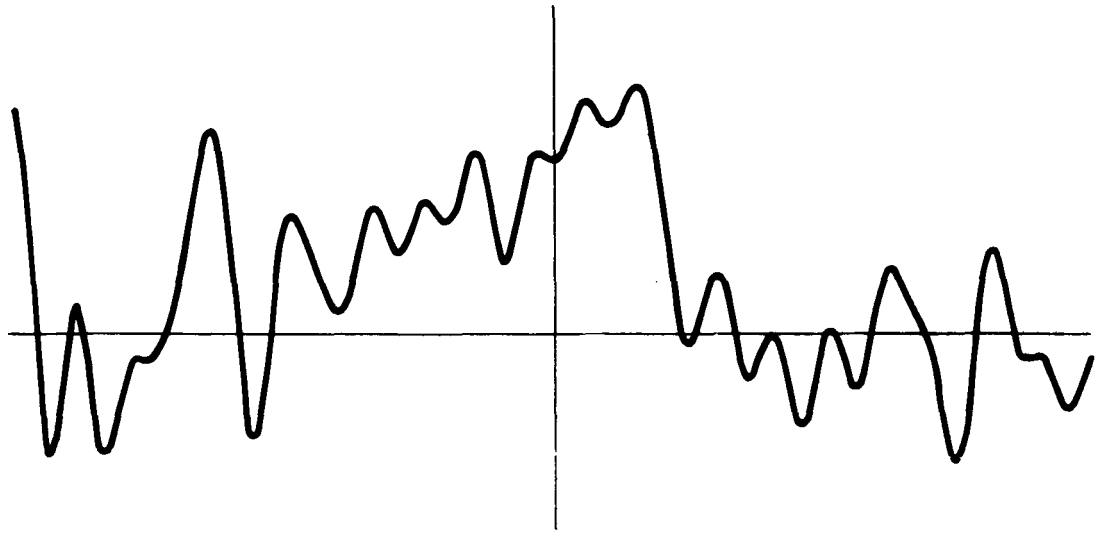

Figure 13. 20 - 30°.

The quasi-specular component is peaked a few degrees toward higher longitudes but falls off steeply toward still higher longitudes; the centroid extends some 5 - 10° toward smaller longitudes. The displacement of the peak is due to the nearby Niliacus Lacus, which has good alignment; the low-frequency tail is attributed to the segment of Deuteronilus between 10 and 20° longitude, which has fair to poor alignment.

There exist two low-frequency satellite peaks of questionable reality, corresponding to longitudes of about 5° and about 355°. The Western and Eastern inlets (F and E) of Dawes' Forked Bay in Meridiani Sinus have appropriate longitudes and alignment, but the required slopes, $\sim 35°$, are very steep.

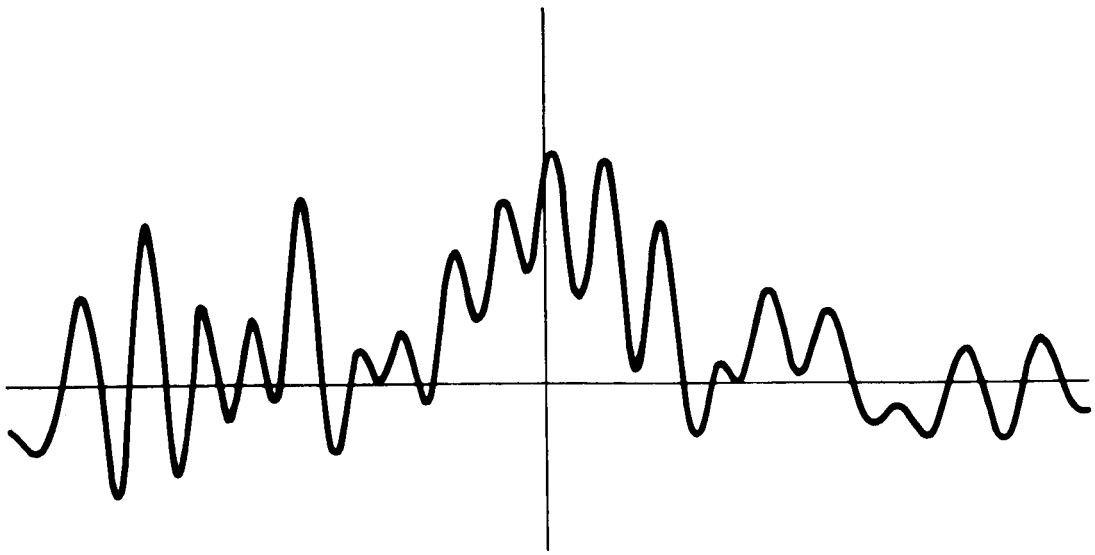

Figure 14. 30 - 40°.

The quasi-specular component here is symmetrical to within the error of measurement. The total power is relatively low, despite the passage of the subterrestrial point through Niliacus Lacus, because the slopes of this dark area deflect specular reflection from the Earth. There are no significant satellite peaks on this (noisy) spectrogram.

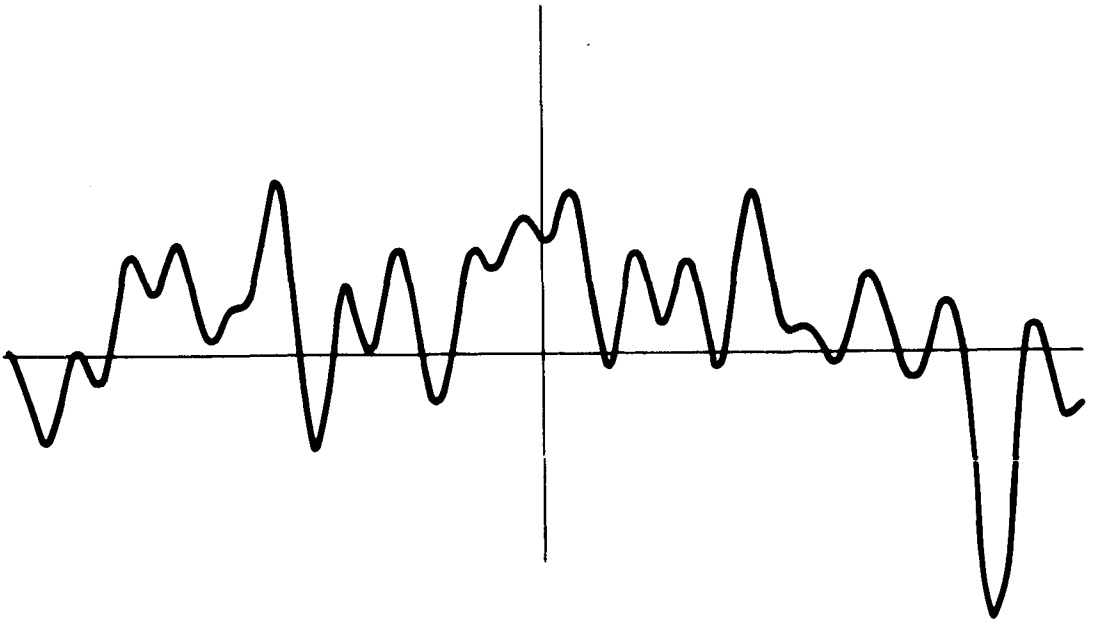

Figure 15. 40 - 50°.

The high-frequency negative spike on this spectrogram illustrates the magnitude of possible random fluctuations produced when the signal-to-noise ratio is low. The centroid of the quasi-specular component has a low-frequency asymmetry explicable in terms of the western slopes of Niliacus Lacus, which have good alignment. Considering the proximity of Niliacus Lacus, we must attribute the low total power in this spectrogram and relative insignificance of the low-frequency tail to general slopes on the western ramparts of Niliacus Lacus $> 8°$ or $\sim 0°$. There is no clear satellite peak due to well-aligned Nilokeras, either because of too steep or too shallow a slope.

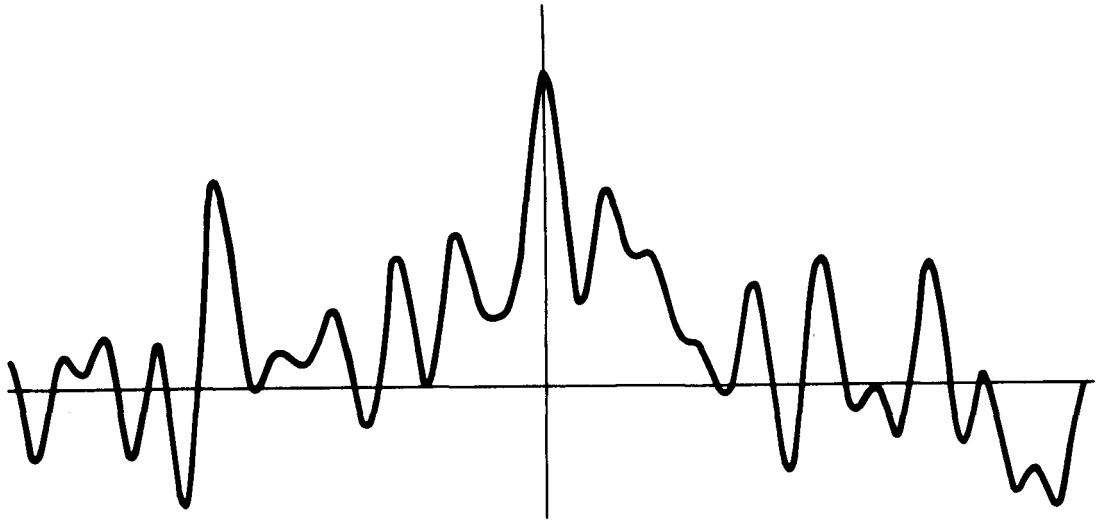

Figure 16. 50 - 60°.

The relative maximum in total power for this longitude range is attributed to the southern slopes of Nilokeras, which was very dark in 1965 (cf. Figure 1). The quasi-specular component is symmetrical about the subterrestrial point; Nilokeras is also distributed symmetrically and is aligned well. The comparison between this spectrogram and the last suggests that the western slopes of Nilokeras are very shallow. Were dark areas lowlands this spectrogram would be difficult to explain; the far side of Nilokeras is poorly aligned, and the required slopes would be ~10° .

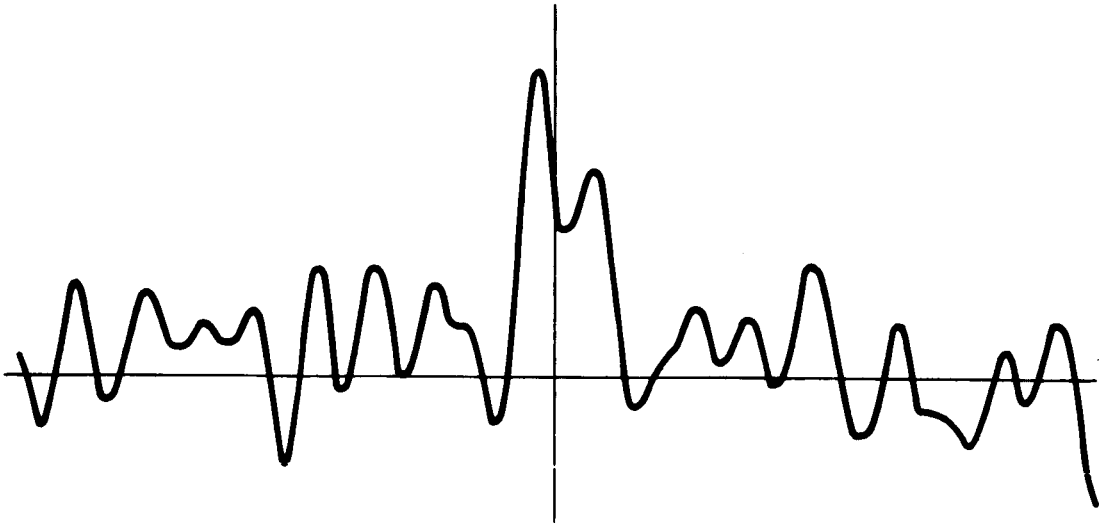

Figure 17. 60 - 70°.

From this longitude to 140°, the total power is low (Figure 3) and there are no prominent dark areas (Figures 1 and 2). In this spectrogram the quasi-specular component is symmetrical, within the probable error, about the subterrestrial point, which falls in the Tractus Albus desert. Lunae Palus probably contributes. There is no significant low-frequency indication of the the western ramparts of Nilokeras, suggesting they are steeper than ~8°, or shallower than ~2°. Comparison with the preceding spectrogram suggests the shallow alternative.

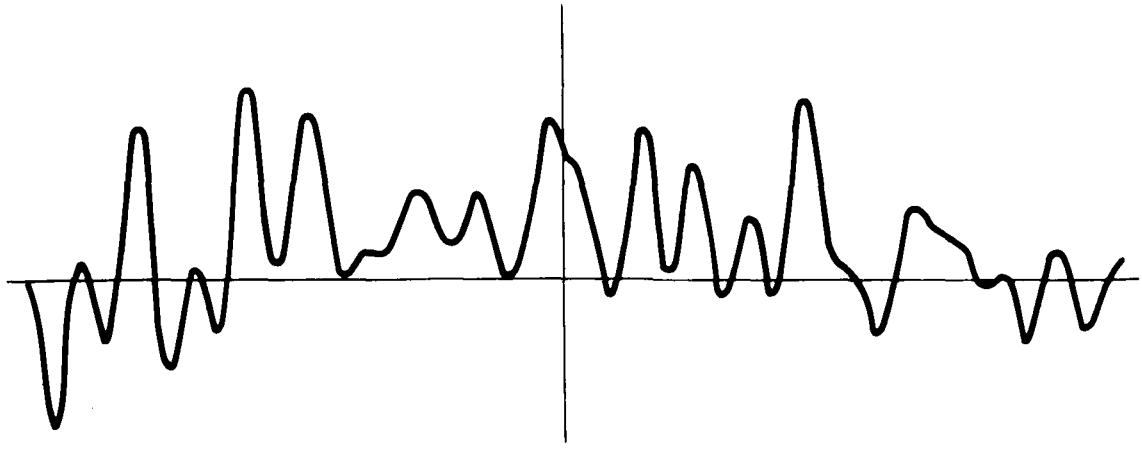

Figure 18. 70 - 80°.

Symmetrical quasi-specular component: Tractus Albus desert. No high-frequency sign of Ceraunius or low-frequency sign of Lunae Palus. Although aligned well, these dark areas were not prominent in 1965 (see Figure 4).

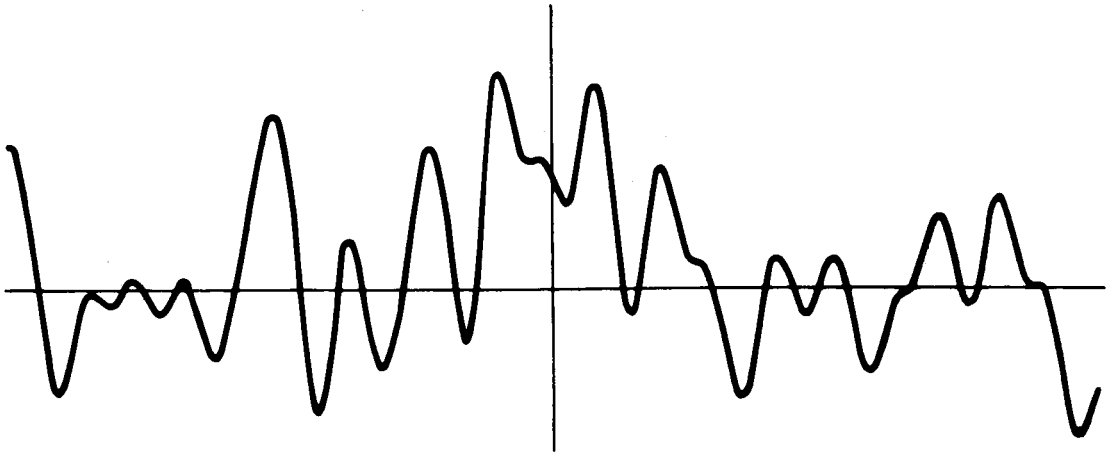

Figure 19. 80 - 90°.

Same remarks as for previous spectrogram.

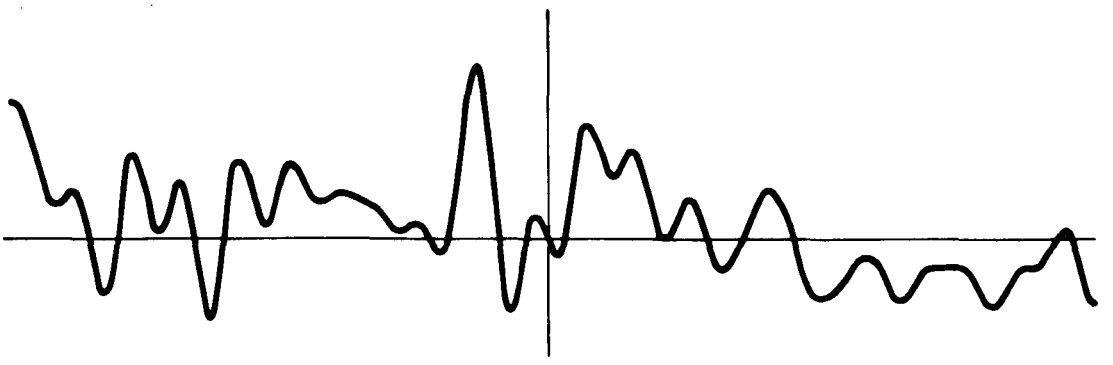

Figure 20. 90 - 100°.

This spectrogram has the lowest power return of all 36. There is no clear quasi-specular component at all, although it possibly might be the feature shifted some 4° to smaller longitudes. The fact that the reflectivity is significantly less here than in such bright areas as Tractus Albus or Elysium must be explained. This is the clearest case in the set of 36 spectrograms in which the subterrestrial point swept through (rather than passed near) a narrow classical "canal" of some darkness, Ceraunius [compare Figure 2 with the end-map of Slipher (1962)]. If such features have steep slopes normal to their long dimensions, then a minimum in radar reflectivity is expected when they are at the subterrestrial point.

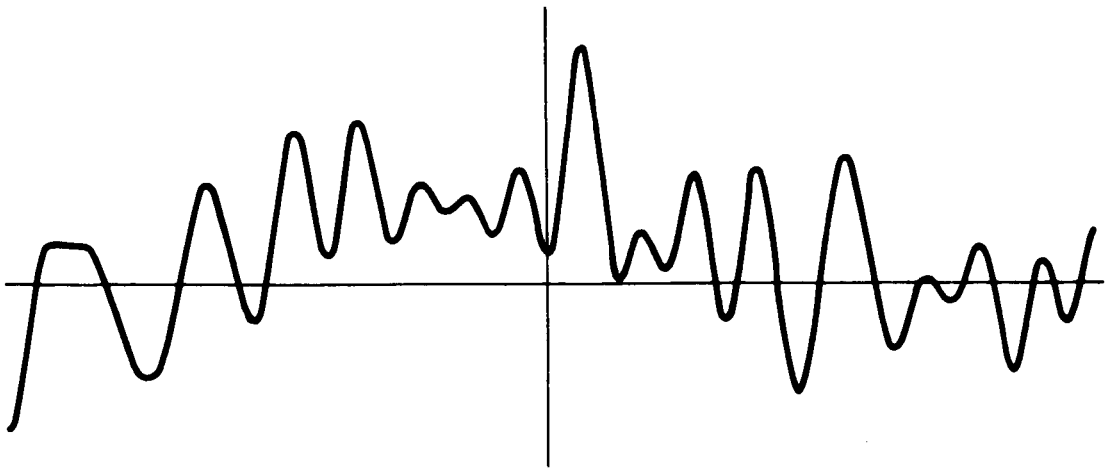

Figure 21. 100 - 110°.

Within the probable error, symmetrical quasi-specular component. Some sign of a low-frequency tail, attributable apparently uniquely to Ceraunius.

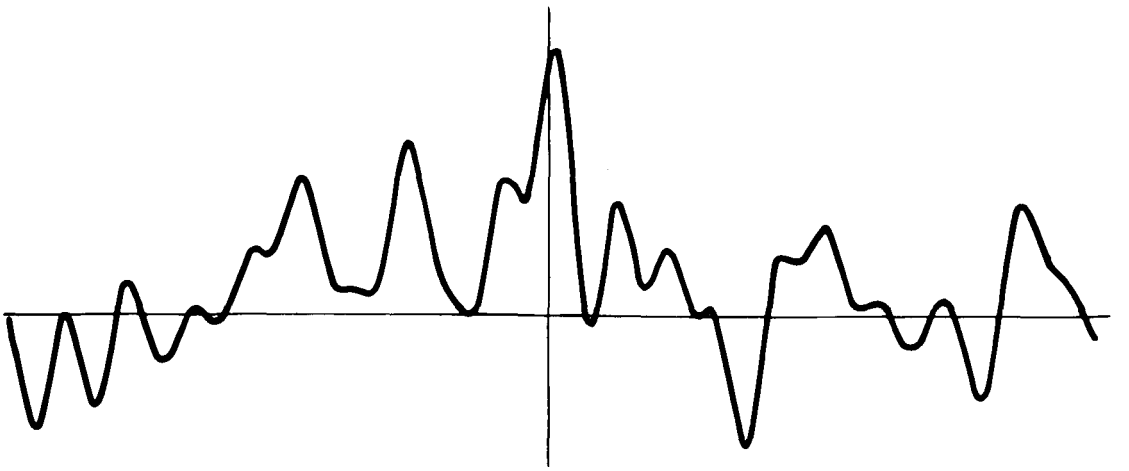

Figure 22. 110 - 120°.

Peak of quasi-specular component symmetrical about subterrestrial point. The dark area Tantalus is properly positioned and aligned. There is a suggestion of a low-frequency tail, with displacements corresponding approximately to the position of Ceraunius; if so, this feature would have slopes ~ 12° on its western ramparts.

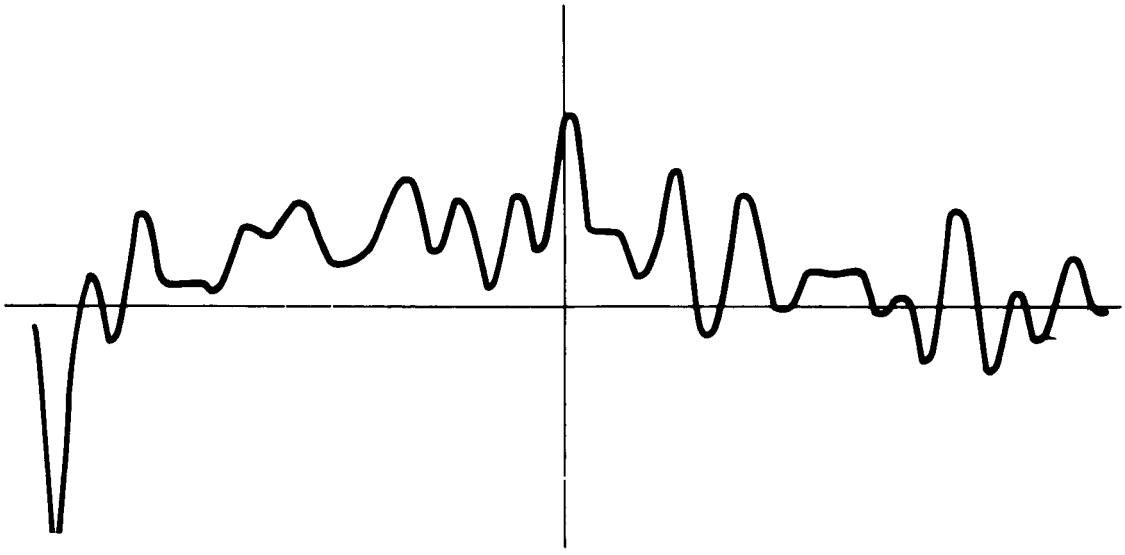

Figure 23. 120 - 130°.

Symmetrical quasi-specular component. Note that this and the next spectrogram are in the region of the bright area Nix Olympica; yet no significant low-frequency feature appears here, or high-frequency feature on the next spectrogram, as might be expected if Nix Olympica were characterized by changing slopes. Neither is there a marked decline in total power, as would be expected if Nix Olympica were a steep elevation.

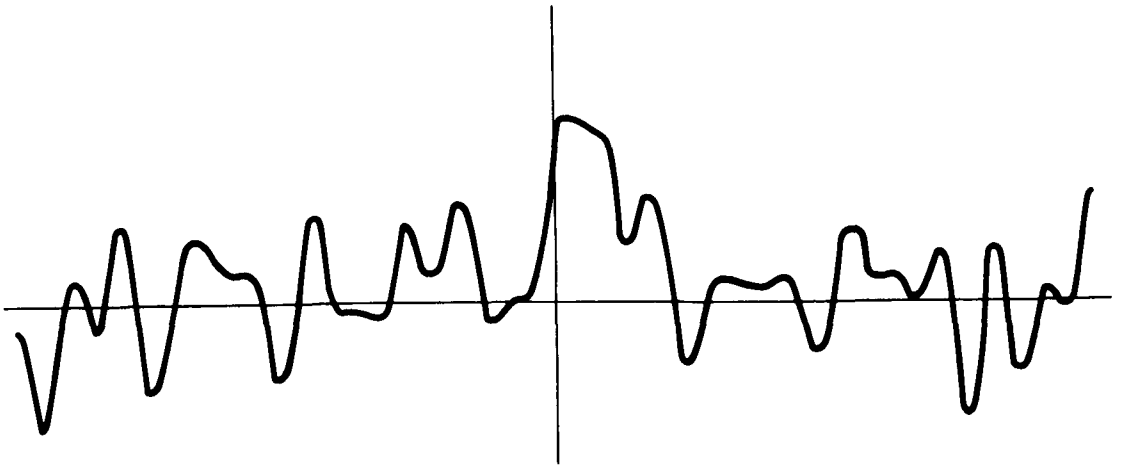

Figure 24. 130 - 140°.

Both the peak and the centroid of the quasi-specular component are shifted to higher longitudes. Southern Pyriphlegethon, the dark area just west of Nix Olympica, and Phlegethon, the dark area just north of it, are suitably positioned and have good alignment.

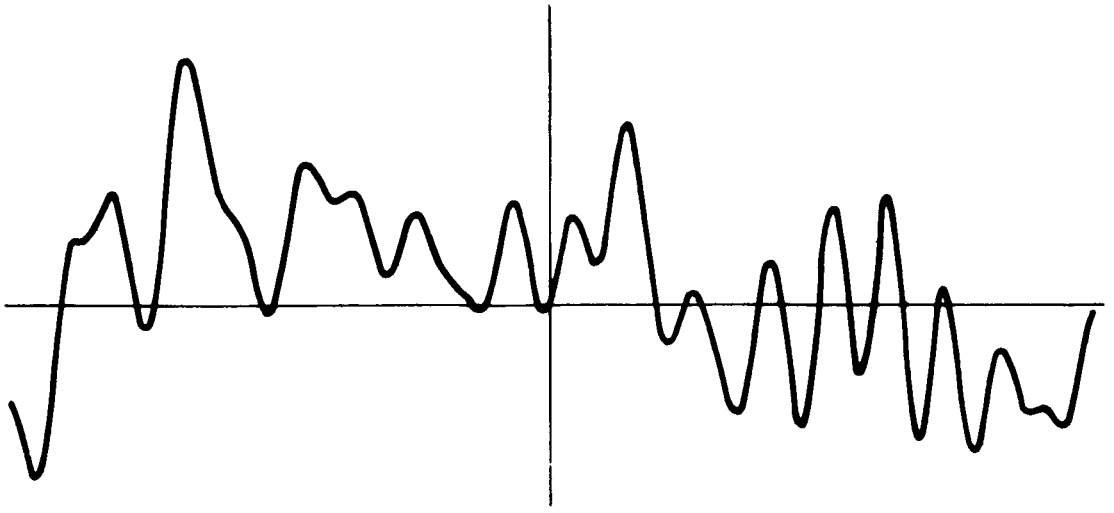

Figure 25. 140 - 150°.

There is no clear quasi-specular component on this noisy spectrogram. A maximum displaced a few degrees to higher longitudes and a centroid displaced to lower longitudes are possible but by no means clear. The total power is low as the subterrestrial point passes through Pyriphlegethon.

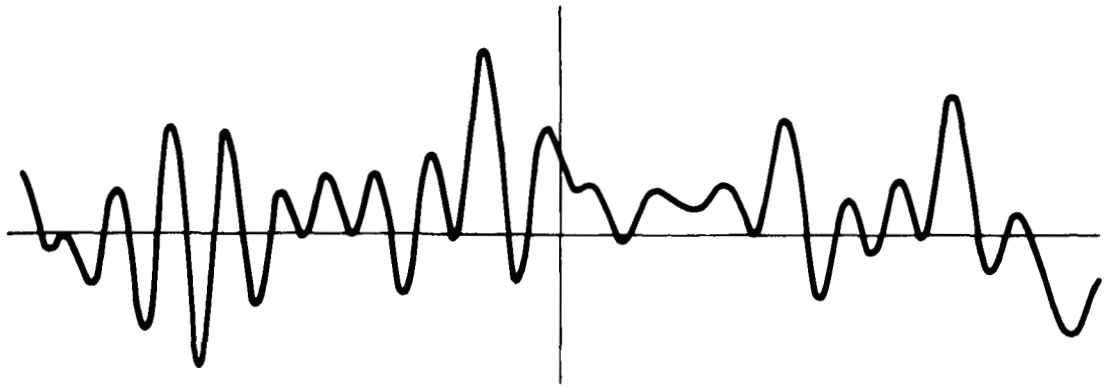

Figure 26. 150 - 160°.

There is no clear quasi-specular component on this noisy spectrogram. There is some possibility that the maximum and the centroid are both displaced several degrees to lower longitudes, corresponding to Pyriphlegethon, which is properly positioned and aligned. Its slopes would then be 3 - 8°.

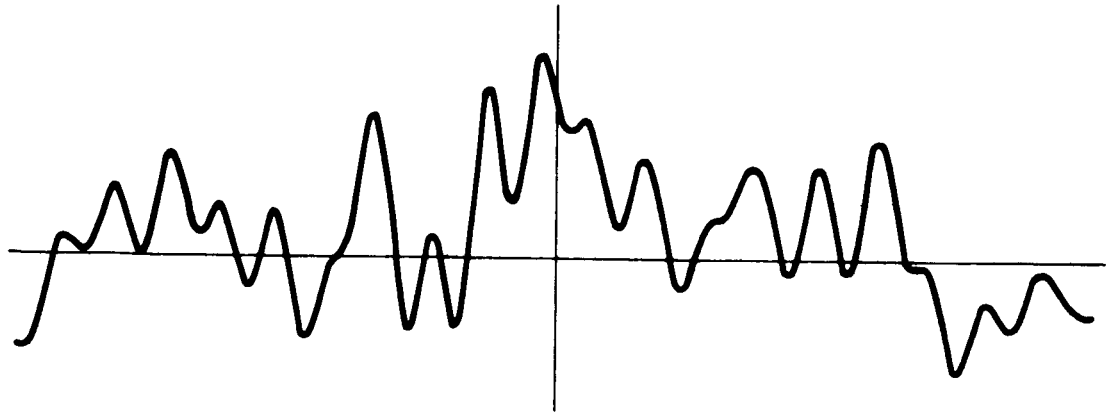

Figure 27. 160 - 170°.

Symmetric quasi-specular component. The subterrestrial point passes just south of the symmetrically arranged dark area Titanum Fons, which accounts for the increase in power.

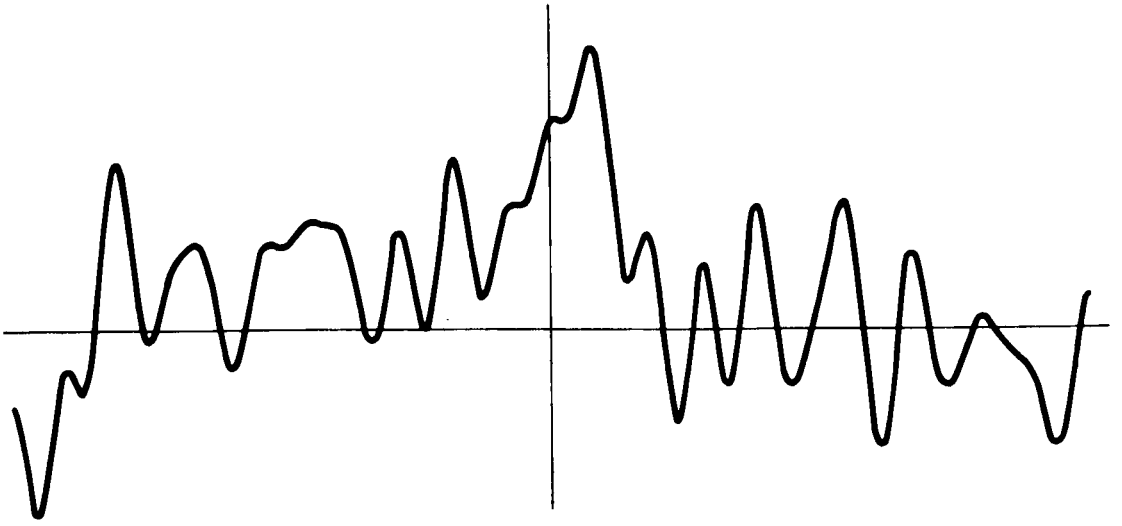

Figure 28. 170 - 180°.

Within the probable errors, a symmetric quasi-specular component. Titanum Fons is still arranged symmetrically about the subterrestrial point.

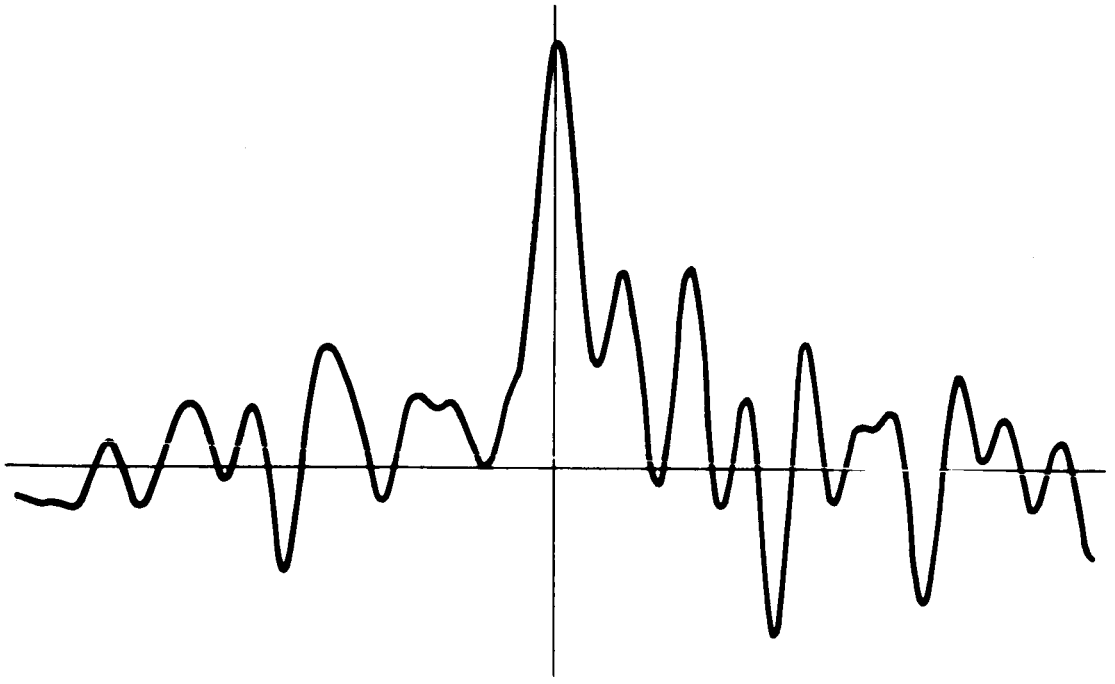

Figure 29. 180 - 190°.

Although the total power has not increased on this spectrogram, the quasi-specular component is narrower and somewhat more pronounced. There are no significant dark areas intercepted by the subterrestrial point; but the high-frequency asymmetry of the centroid immediately indicates that Trivium Charontis is involved. Its position and alignment are fair and can explain the asymmetry and modest power return. Subsurface extensions of Trivium Charontis may be suitably sloped to contribute to the spike at the subterrestrial point.

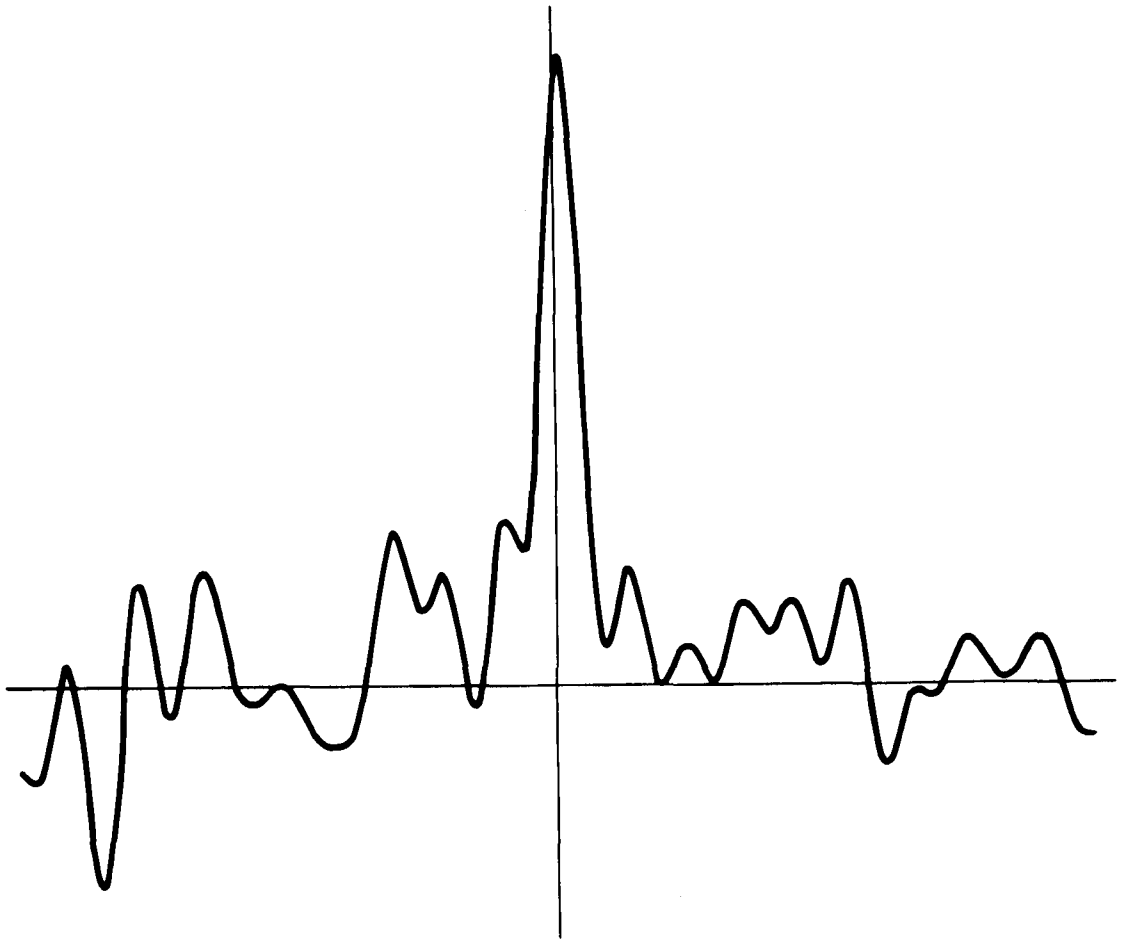

Figure 30. 190 - 200°.

Narrow symmetric high-power quasi-specular reflection. The major contribution comes from the northern tip of Trivium Charontis, which is symmetrically oriented and which must have a very shallow slope, close to 0°. Alignment is fair.

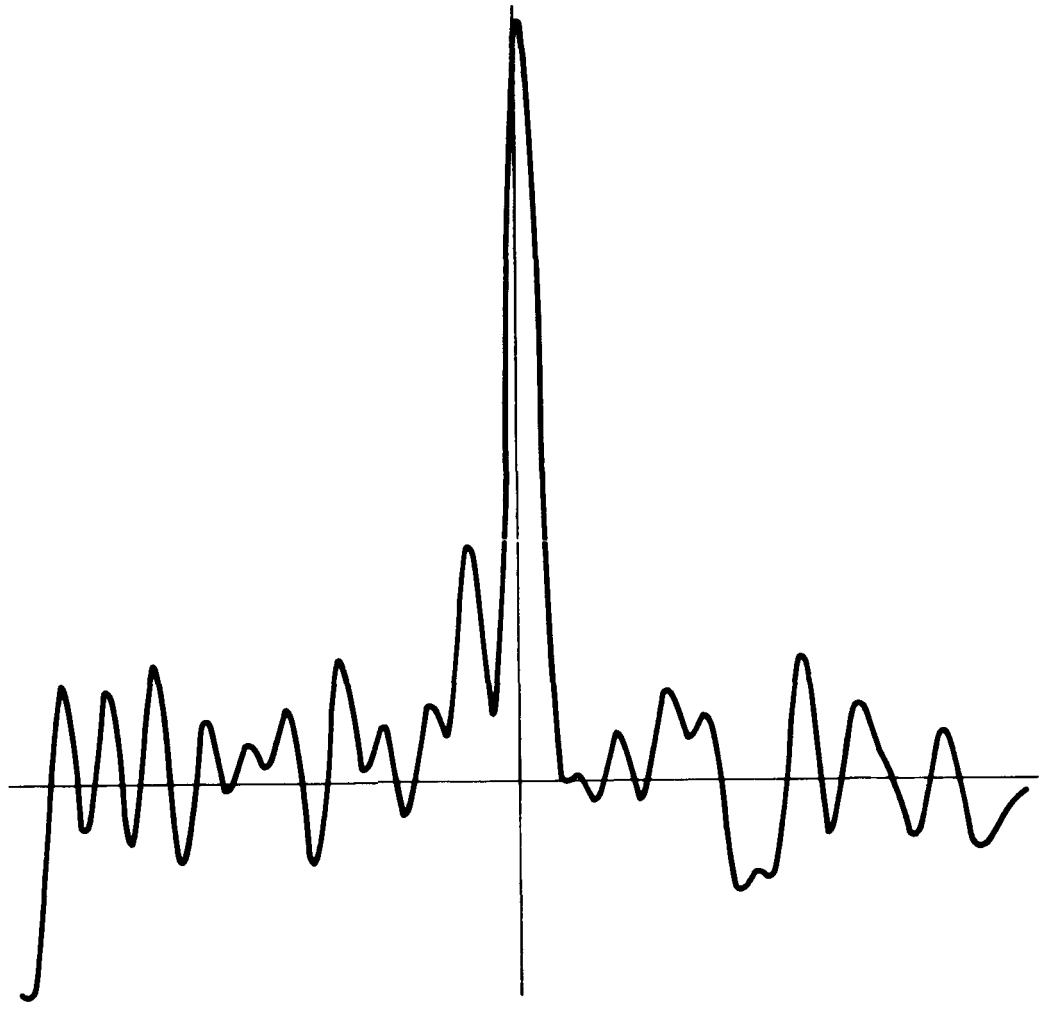

Figure 31. 200 - 210°

Narrow high-power quasi-specular component. The maximum is centered on the subterrestrial point, but the centroid is displaced several degrees to lower longitudes. The subterrestrial point falls in the Elysium desert. It is a very high-power return, peaked at 201° longitude in the Arecibo data set; i.e., within a few degrees of the adjacent Trivium Charontis, which is very well aligned. The central maximum is attributed to the subsurface slopes of Trivium, and to the northern ramparts of Trivium and of Cerberus, just south of the subterrestrial point. The low-frequency asymmetry is due to the western slopes of Trivium. Comparison with the results of the previous spectrogram shows that Trivium Charontis has steeper slopes in its long dimensions than in its short dimension.

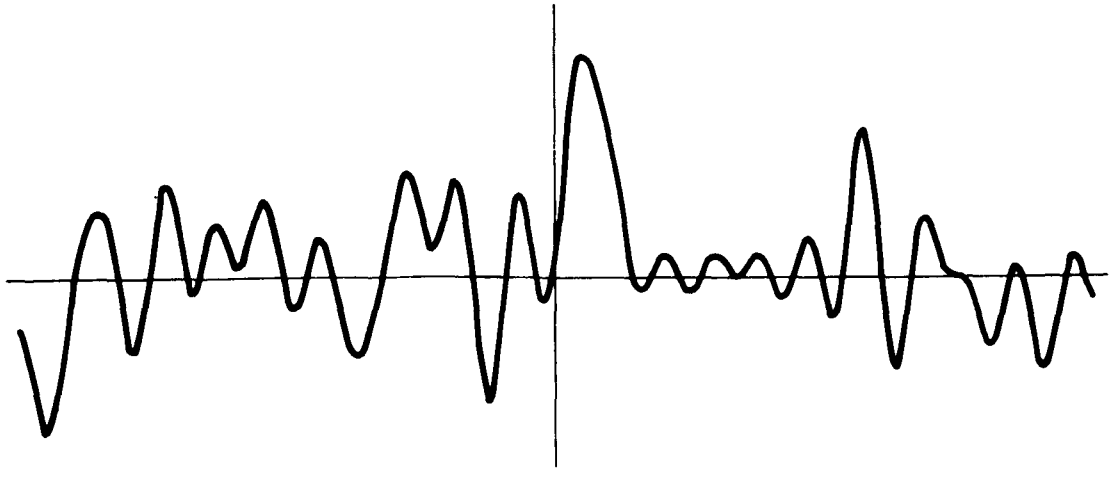

Figure 32. 210 - 220°.

Within the probable error the low-power quasi-specular return is symmetrical about the subterrestrial point, which falls in the Elysium desert. Despite their good alignment, there are no contributions from Trivium Charontis or Cerberus, consistent with the shallow slopes of a few degrees already deduced for Trivium. The reflectivity on this spectrogram is that of a bright area relatively uncontaminated with dark-area contributions.

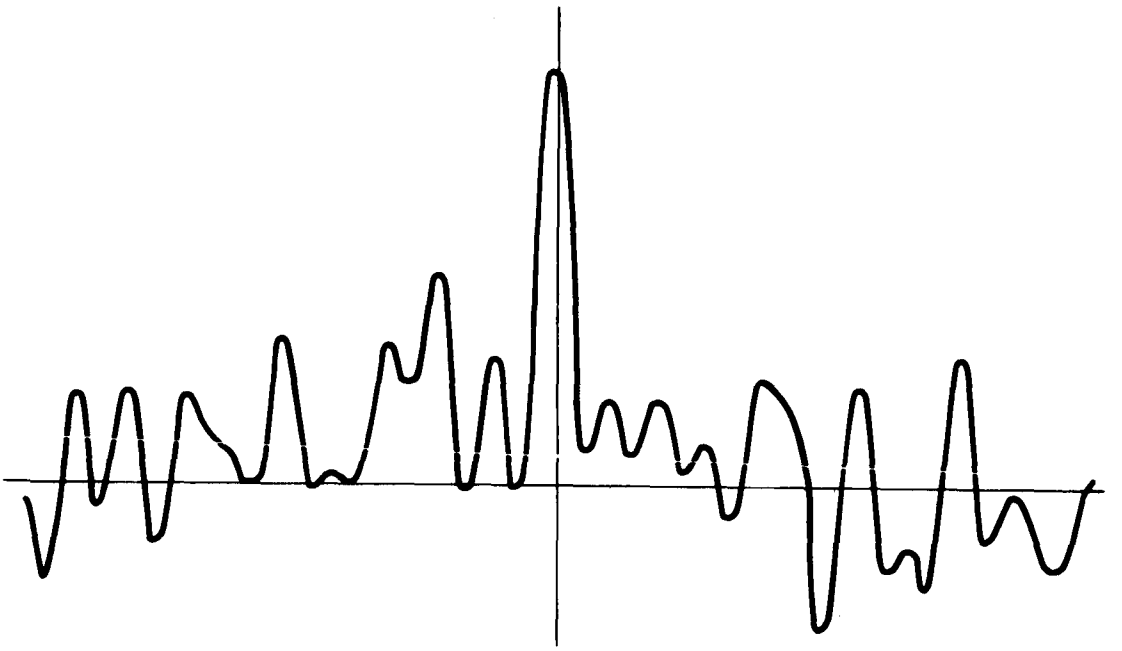

Figure 33. 220 - 230°.

Symmetric low-power quasi-specular component. Subterrestrial point traverses Eunostos, a faint elongated dark area, and mostly encounters darker areas than in the previous spectrogram (see Figure 1).

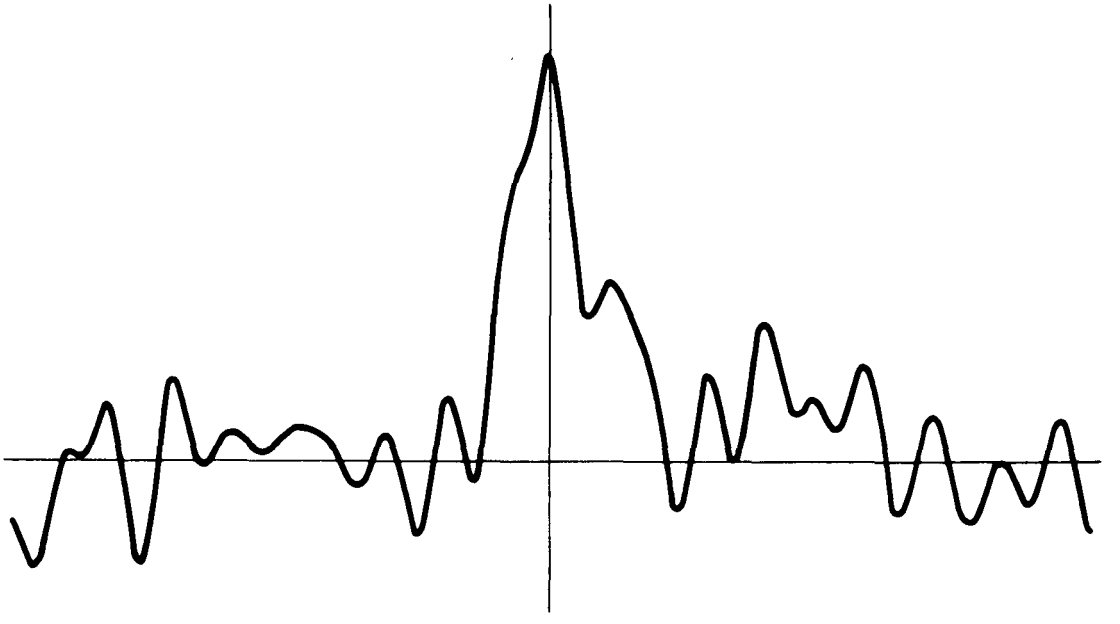

Figure 34. 230 - 240°.

Peak of quasi-specular component centered at subterrestrial point, but there is a distinct high-longitude asymmetry of the centroid, amounting to several degrees. With conventional maps (e.g., Figure 2) this asymmetry would have been inexplicable. But study of the 1965 map (Figure 4) shows the presence of a new dark area, a greatly enhanced Nodus Laocoöntis with approximately the correct longitude and with excellent alignment to account for the asymmetry.

This spectrogram provides another test of the sign of the elevation difference between bright areas and dark areas. If Nodus Laocoöntis were a lowland, the asymmetry would appear at least 12° from the subterrestrial point; but if it is a highland, its near slope may be as little as 3° from the subterrestrial point, in agreement with the spectrogram.

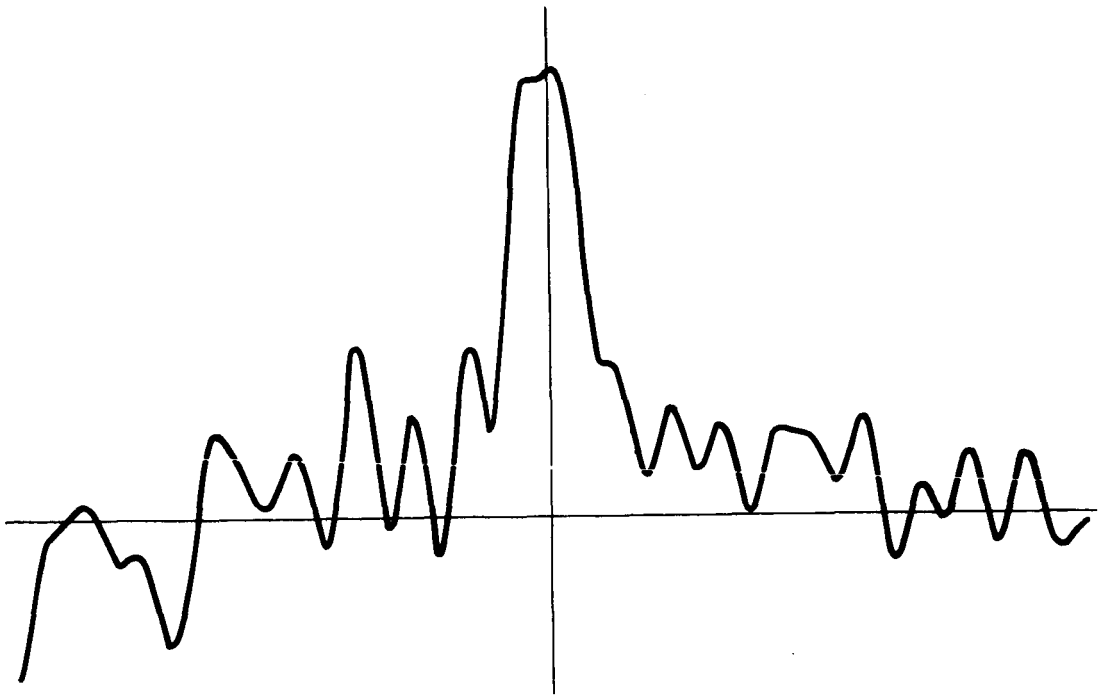

Figure 35. 240 - 250°.

Broad centered symmetric quasi-specular component; this is the longitude interval of maximum total power in the Goldstone observations. The subterrestrial point falls very close to, and then within, the enhanced Nodus Laocoöntis; and part of the quasi-specular component arises from this feature (see arrow in Figure 4). If this is the primary cause of the high reflectivity, it follows that the slopes of the enhanced Nodus Laocoöntis are shallow (~2° or less). Note that no high-frequency satellite owing to Nepenthes appears on this spectrogram.

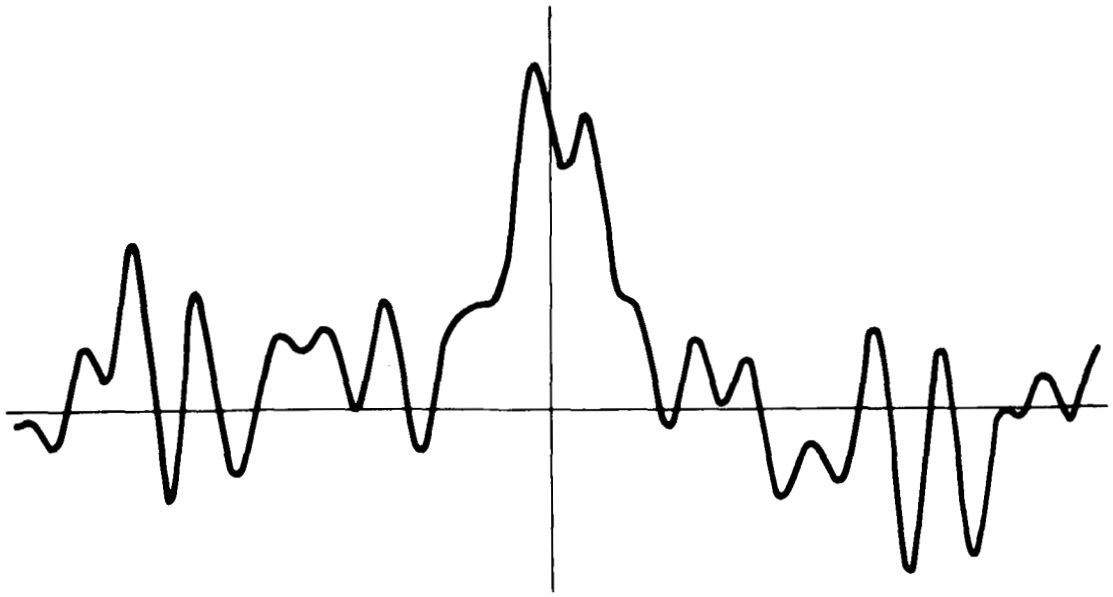

Figure 36. 250 - 260°.

There is no significant low-frequency asymmetry. Despite the hint of a high-frequency shoulder to the peak there is still no clear high-frequency feature due to Nepenthes, despite its favorable alignment. We conclude that the slopes in Nepenthes at latitude 21.°6 are very shallow.

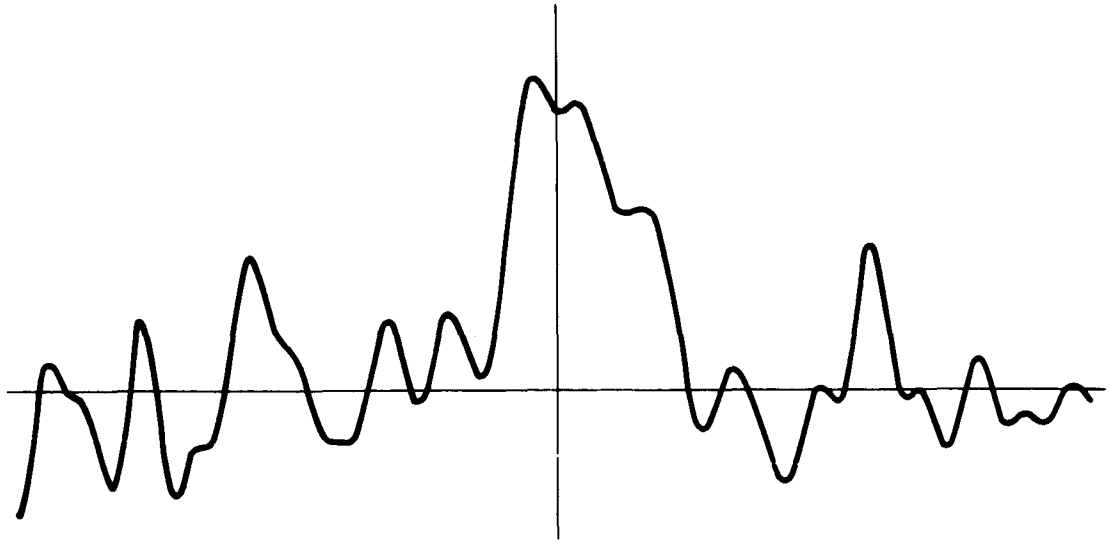

Figure 37. 260 - 270°.

High-reflectivity quasi-specular component with its maximum centered at the central frequency, but with a shoulder skewed to high frequencies, corresponding to a longitude displacement ~5°. The symmetric fraction of the return is attributed primarily to Nepenthes, for which we have already deduced shallow slopes. The asymmetric return, as well as the remainder of the symmetric return, is due to Moeris Lacus, which has good alignment. Note that a high-frequency satellite exists in the position expected for the eastern slopes of Syrtis Major ($\Delta\phi \sim 10°$), but it is not clearly out of the noise.

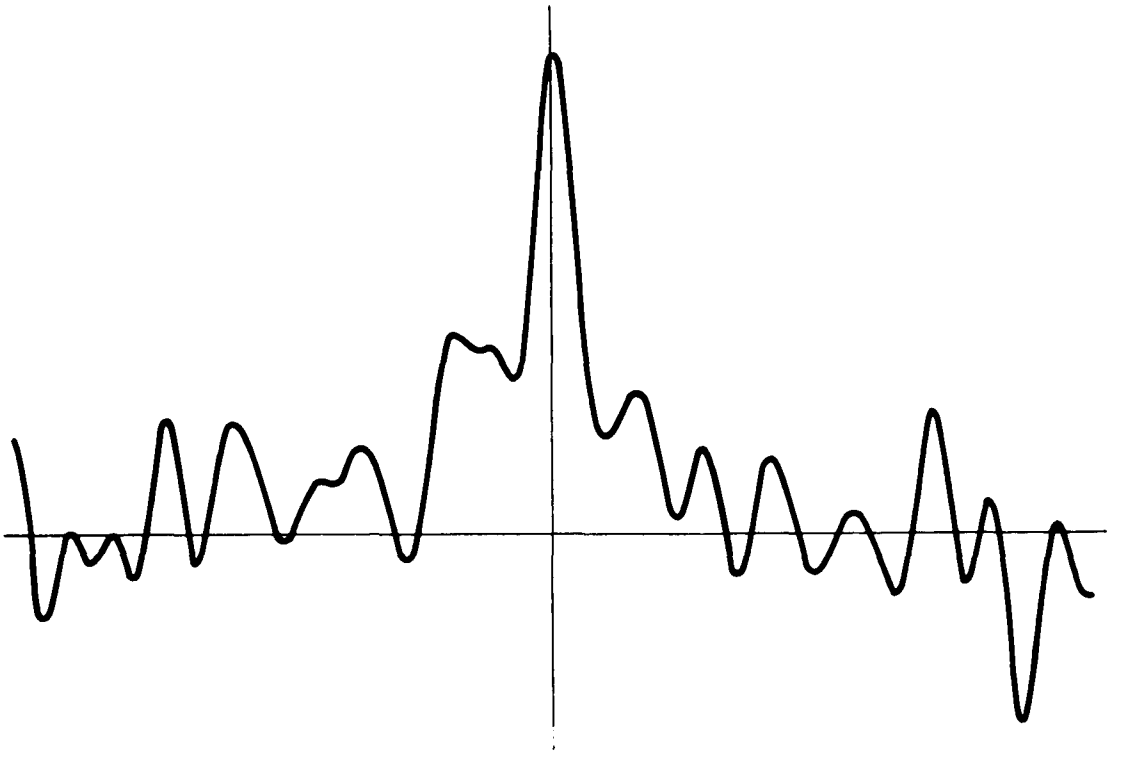

Figure 38. 270 - 280°.

This second-highest power return in the Goldstone observations shows a quasi-specular peak at the central frequency, but both a high-frequency and a low-frequency shoulder. The subterrestrial point here traverses a region surrounded on three sides by well-aligned dark areas. The central peak is due to Moeris Lacus; the low-frequency asymmetry to Moeris Lacus and the western slopes of Nepenthes (required slopes, a few degrees); and the high-frequency asymmetry to the eastern slopes of Syrtis Major (slopes ~4°).

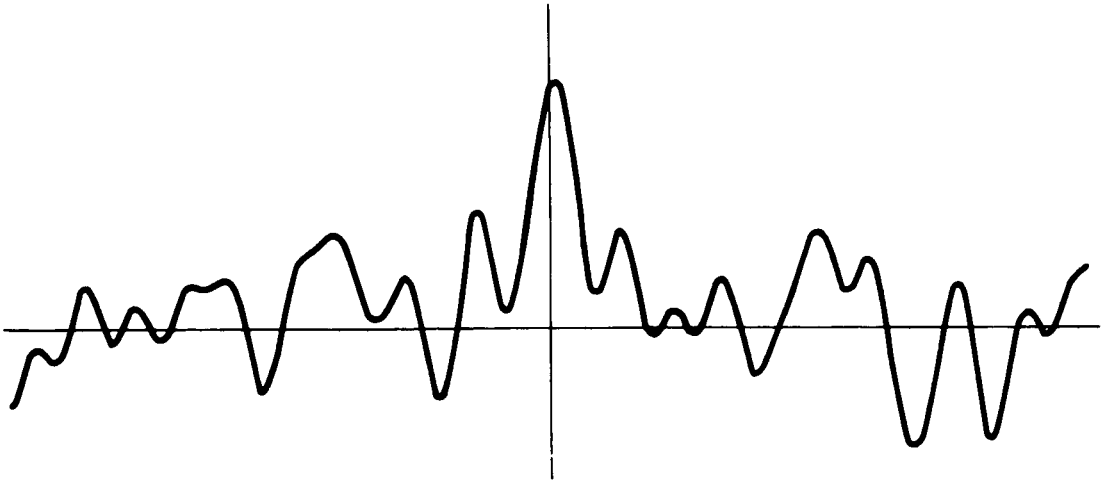

Figure 39. 280 - 290°.

Symmetrical quasi-specular component, and relatively low power, despite the fact that the subterrestrial point is centered on the northern tip of Syrtis Major, one of the darkest Martian dark areas. The low power is explicable in term of high slopes (~4° or more) such as deduced for Syrtis Major from the preceding spectrogram. The slopes should be such that when the subterrestrial point is east or west of Syrtis Major in this spectrogram the backscatter to Earth is small. There are also no properly aligned dark areas nearby.

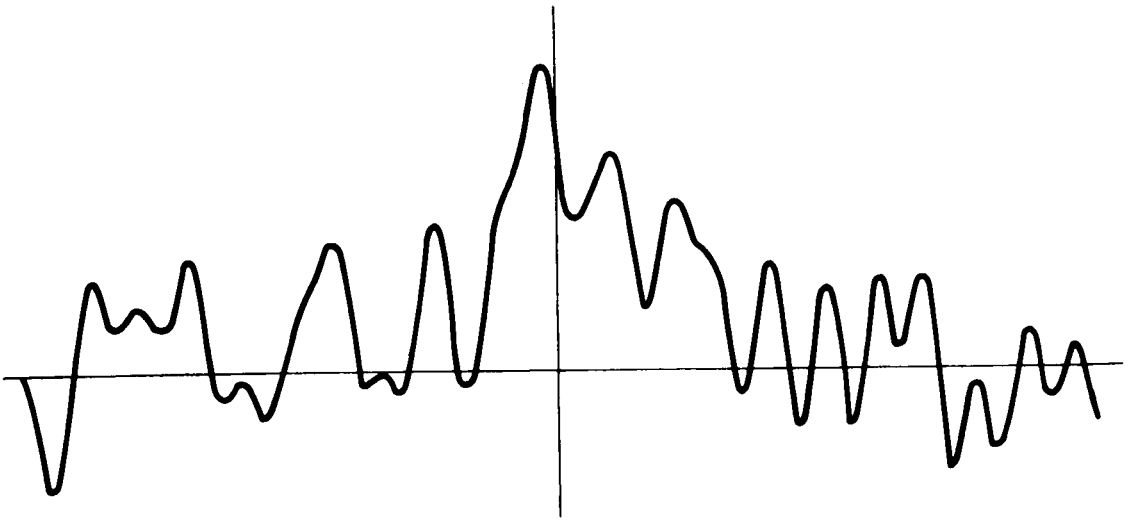

Figure 40. 290 - 300°.

Centroid asymmetric to high frequencies. Power is a local maximum. Both can be attributed to Syrtis Major; its southwestern ramparts have fair alignment. Were dark areas lowlands there would be no plausible explanation of this high reflectivity without assuming slopes of 30 - 50°. The absence of a low-frequency asymmetry implies the western slopes of Syrtis Major are inclined $< 2°$ or $> 7°$. From the results of the preceding spectrum, the latter alternative seems favored.

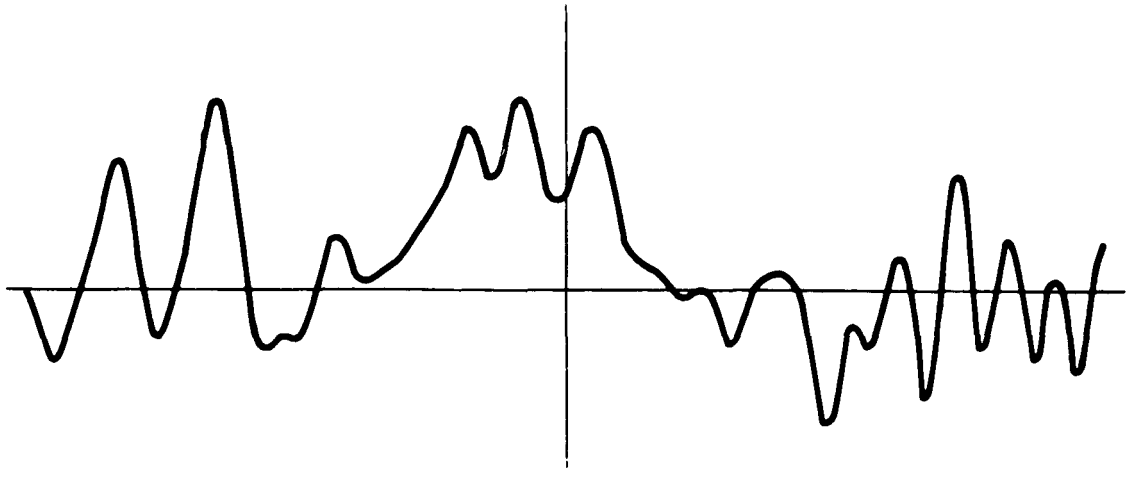

Figure 41. 300 - 310°.

Centroid of quasi-specular component is asymmetric to low frequencies. The southwestern ramparts of Syrtis Major have an appropriate longitude and alignment. Were the far side of Syrtis Major to be the source of the asymmetry — as would be the case if dark areas were lowlands — the longitude shift required would be ~ 20°. There is, in fact, a feature with the corresponding frequency displacement, but it is in the diffuse component of the spectrum, where the noise level is high, and we do not consider it significant.

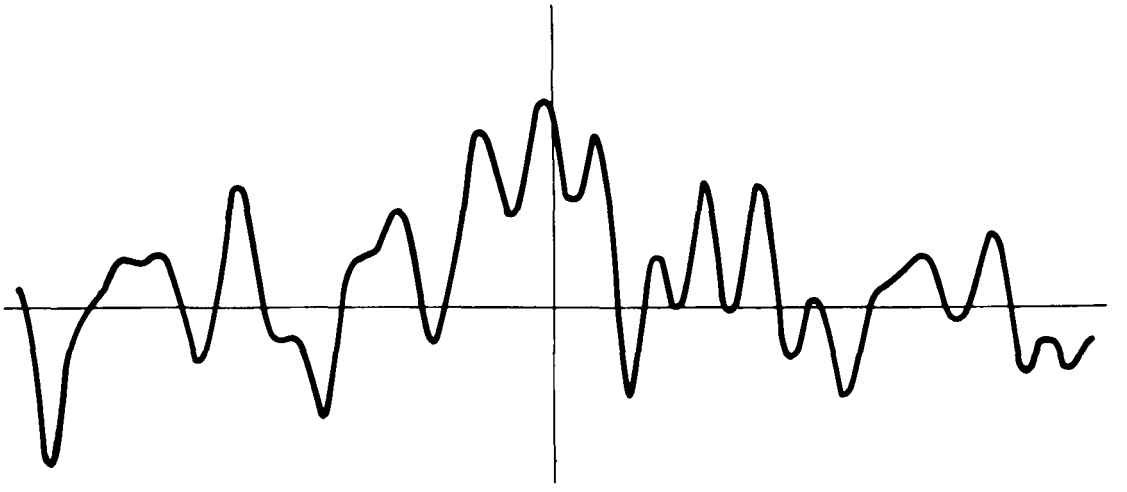

Figure 42. 310 - 320°.

Within the probable error of measurement this is a symmetrical quasi-specular component. The return is attributed to the Arabia desert.

In Table 4, we summarize the major points of the spectral analysis. The equivalent longitude displacement or half-width of each significant spectral feature is displayed, together with the dark area deemed responsible, and a qualitative characterization of the alignment of the dark area. From the dark-area identification an anticipation of the expected longitude displacement is made on the basis of the Martian cartography and the excursion range of subterrestrial points. The agreement between anticipated and observed longitude displacements is seen to be good; but we reemphasize that not all nearby dark areas appear in the spectra, because of slopes and alignments. A prediction of spectral features cannot be made without some prior knowledge of the prevailing slopes. These deduced slopes are given in the last column of Table 4, from the planetocentric angular distance between subterrestrial points and dark areas responsible for spectral features.

Table 4. Comparison of principal observed and anticipated spectral features.

Longitude range	Spectral feature	Observed longitude displacement or half-width	Dark area responsible	Alignment	Anticipated longitude displacement	Required slope
350-360°	High-frequency asymmetry of centroid	0-4°	S. slopes, Deuteronilus	good	0-4°	9 ± 3°
0-10°	High-frequency asymmetry	0-6°	S. slopes, Deuteronilus	fair	0-4°	6 ± 3°
10-20°	Symmetric central spike	3°	S. slopes, Deuteronilus	good	0-8°	5 ± 2°
20-30°	High-frequency shift, central spike	2-6°	S. slopes, Niliacus Lacus	good	1-3°	3 ± 2°
	Low-frequency tail	0-22°	S. slopes, Deuteronilus and S. slopes Niliacus Lacus	fair	0-~ 10°	2 to ~20°
30-40°	Symmetric centroid, low power	7°	Niliacus Lacus	-	0-10°	> 4°
40-50°	Low-frequency asymmetry of low power	0-4°	W. slopes Niliacus Lacus	good	0-7°	~0° or ≥ 8°
	Absence of high-frequency satellites	-	S.E. slopes Nilokeras	good	8-16°	< 7° or > 13°
50-60°	Narrow central spike	2°	S. slopes Nilokeras	good	1-4°	3 ± 2°
	Absence of low-frequency satellite	-	W. slopes Niliacus Lacus	good	8-18°	< 8°
60-70°	Absence of low-frequency satellite	-	W. slopes Nilokeras	good	0-8°	> 8° or < 2°
90-100°	Low power	-	E. and W. slopes, Ceraunius	-	-	> 5°
100-110°	Low-frequency satellite	0-18°	W. slopes Ceraunius	good	3-15°	0 to 18°
110-120°	Symmetric central spike	2°	Tantalus	-	0-4°	2 ± 2°
	Low-frequency asymmetry of centroid	2-17°	W. slopes Ceraunius	good	5-20°	2 to 17°
160-180°	Symmetric centroids	0-4°	S. slopes Titanum F.	good	0-3°	2 ± 2°
180-190°	High-frequency asymmetry of centroid	3-11°	E. slopes, Trivium Charontis	fair	2-12°	3 to 11°
190-200°	Narrow symmetric high-power spike	2°	N. slopes Trivium Charontis	good	2-6°	0 ± 2°
200-210°	Narrow symmetric high-power spike	3°	N.W. slopes Trivium Charontis and of Cerberus	good	2-6°	2 ± 1°
	Low-frequency asymmetry of centroid	2-5°	W. slopes Trivium Charontis	fair	2-12°	4 ± 2°
230-240°	High-frequency asymmetry	3-6°	E. slopes N. Laocoontis	good	3-13°	4 ± 2°
240-250°	Broad symmetric spike	4°	Internal boundaries of N. Laocoontis	good	1-5°	2 ± 2°
250-260°	Absence of high-frequency asymmetry	-	E. slopes Nepenthes	good	0-7°	0 ± 1°
260-270°	Broad central spike	3°	N.W. slopes Nepenthes	good	0-5°	2 ± 2°
	High-frequency asymmetry of centroid	0-6°	N.E. slopes Moeris Lacus	fair	0-9°	5 ± 4°
270-280°	Symmetric high-power central spike	2°	N. slopes Moeris Lacus	good	0-3°	7 ± 3°
	Low-frequency asymmetry	3-6°	N.E. slopes Moeris Lacus	good	3-6°	6 ± 3°
	High-frequency asymmetry	3-6°	E. slopes Syrtis Major	good	1-11°	4 ± 2°
280-290°	Symmetric low-power central spike	2°	Slopes of N. tip Syrtis Major	-	0-10°	> 3°
290-300°	High-frequency asymmetry of centroid	0-8°	N.W. slopes Syrtis Major	fair	0-5°	5 ± 2°
	Absence of low-frequency asymmetry	-	W. slopes Syrtis Major	good	0-6°	< 2° or > 7°
300-310°	Low-frequency asymmetry	2-9°	W. slopes Syrtis Major	fair	5-15°	7 ± 3°

6. RESULTS

From the spectral results of Table 4 it is possible to deduce rough values of $\bar{\alpha}$ and of $\Delta\alpha$ for several Martian dark areas. The slopes of Table 4 deduced from central spikes of dark areas near the subterrestrial point are a measure of $\Delta\alpha$. Slopes deduced from centroid asymmetries, shifts in central peaks, and satellite peaks for the same geometry lie between $\bar{\alpha} + \Delta\alpha$ and $\bar{\alpha} - \Delta\alpha$. When the subterrestrial point is on the dark area, the slopes of Table 4 are a measure of $\Delta\alpha$. Low power returns in this case imply $\bar{\alpha} + \Delta\alpha$ sizable, and $\Delta\alpha$ comparable to $\bar{\alpha}$; both are probably at least several degrees. In all cases in which the alignment is not good the slopes tend to measure $\Delta\alpha$. If a region shows high reflectivity when under the subterrestrial point, then $\bar{\alpha} < \Delta\alpha$.

Consider the region 230-260° around Nodus Laocoöntis. The broad spike at 240-250° with half-width at half maximum of 4° implies $\Delta\alpha \simeq 4°$. The existence of a power maximum at 240-250° implies $\bar{\alpha} < \Delta\alpha$. The slopes deduced from the asymmetry at 230-240° are $4 \pm 2°$, and must lie between $\bar{\alpha} + \Delta\alpha$ and $\bar{\alpha} - \Delta\alpha$. Thus $\bar{\alpha} \simeq 2°$, consistent with both $\Delta\alpha$ and the inequality on $\bar{\alpha}$ above. In the 1963 radar observations, the swath at 13.6 passed through a gap in Nodus Laocoöntis (see arrow, Figure 4). This corresponds to a relative maximum in the returned power (see Table 2), is consistent with the idea of the dark areas as highlands, and is inconsistent with the alternative. Very low mean slopes are indicated, consistent with the 1965 results. A summary of similar estimates for the other dark areas of Table 4 for which such an analysis can be performed is exhibited in Table 5.

The heights of the Martian elevations above the surrounding deserts can be estimated as follows : Let $2\,\Delta\theta_{max}$ be the planetocentric angular width of the elevation in the direction of the mean slope. On the average, $\Delta\theta_{max}$ will be a measure separately of the widths of both the up and the down slopes. Since $\bar{\alpha}$ is the mean slope, the highest point in the elevation — presumed near the center of the feature — is given by

$$h_{max} = R_{\sigma}\,\bar{\alpha}\,\Delta\theta_{max} \quad . \tag{3}$$

Table 5. Roughly estimated values of $\bar{\alpha}$ and $\Delta\alpha$ for selected Martian dark areas.*

Area	$\bar{\alpha}$	$\Delta\alpha$
Deuteronilus	>3°	6°
Niliacus Lacus	3°	2°
Ceraunius	>4°	6°
Trivium Charontis	2°	3°
Nodus Laocoöntis	2°	4°
Nepenthes	1°	1°
Moeris Lacus	3°	6°
Syrtis Major	4°	5°

*Associated probable errors are at least 50%.

Through a numerical coincidence, the observed value of the planetary radius and the conversion from radians to degrees yields

$$h_{max} \simeq \bar{\alpha}\,\Delta\theta_{max} \quad ; \tag{4}$$

here h_{max} is measured in kilometers and these angles in degrees. The actual maximum altitudes of the dark areas may be less than given by equation 4, depending on whether their triangular cross sections are truncated. Weathering will, of course, tend to flatten ridges, but since, in the absence of liquid water on the Martian surface, erosion should be much less efficient than on Earth, substantial truncation may be less common than on Earth. Further, if the tops of elevations were generally flat, many of the features we have discussed -- e. g., the 10° displacement of radar-reflection maximum from the centers of dark areas — would no longer be explicable. In a few cases, most noticeably Deuteronilus and Moeris Lacus, values of $\bar{\alpha}$ have been deduced in Table 5, although the subterrestrial point has not passed through the region. In these cases it is possible for the tops to be flat without generating contradictions. Comparison of the 1963 and 1965 power spectra (cf. Figs. 1 and 2) shows a relative maximum of the radar reflectivity on the slopes of Syrtis Major in 1963, but not in 1965. Were the northern boundaries of Syrtis Major sloped, but its central regions truncated, this result would be explicable. Moreover, the general slopes of principal dark areas such as Syrtis Major cannot extend to their centers without exceeding the strengths of common materials (see below).

The resulting maximum elevations are given in Table 6. Except possibly for Deuteronilus and Moeris Lacus, the highest altitudes are probably not much less than the values of h_{max}. Note, however, that the estimates of h_{max} have probable errors of 50% or more, because of the errors in deriving $\bar{\alpha}$. Deuteronilus and Ceraunius seem to have a smaller extent when observed visually. In fact, Deuteronilus has been observed as a double canal during springtime in the Northern Hemisphere. As a result the values of $\Delta\theta$ derived from the map for these features may be overestimates.

Table 6. Estimated heights of highest points for selected Martian dark areas.*

Area	$\bar{\alpha}$	$\Delta\theta_{max}$	h_{max}(km)
Deuteronilus	>3°	<2°	~6
Niliacus Lacus	3°	5°	15
Ceraunius	>1°	<1.5°	~6
Trivium Charontis	2°	2.5°	5
Nodus Laocoöntis	2°	3.5°	7
Nepenthes	1°	4°	4
Moeris Lacus	3°	5.5°	≤16.5
Syrtis Major	4°	3°	12

*Associated probable errors are at least 50%.

From the above discussion we have concluded that the dark areas on Mars are highlands. We now briefly review the criteria and examples used to arrive at this conclusion. All criteria are based on the fact that the near side of a highland and the far side of a lowland, relative to the subterrestrial point, will backscatter radiation to the observer. The frequency displacement of satellites from the center frequency and the displacement of the centroid or peak of the quasi-specular component allow an estimate of the longitude displacement of the feature responsible. The radar returns for the Martian longitude intervals 230-240°, 300-310°, and 20-30° illustrate this criterion. In these cases the far sides of the dark areas are too far away to account for the feature. A second method to distinguish the highland from the lowland hypothesis is estimating the required slope in each

case. When the dark areas are responsible for a significant enhancement of the quasi-specular power, such deduced slopes must be typical. Very large slopes, 10-30°, are found under the assumption the dark areas are lowlands, while much more moderate slopes are found if the dark areas are highlands. As we will see below, average slopes of between 10 and 30° are inadmissable since they lead to features that cannot be mechanically supported. The longitude intervals 270-280°, 290-300°, and 50-60° illustrate this method. Finally the lowland hypothesis sometimes requires a larger half-width to the quasi-specular component than is observed. The regions 200-210° and 20-30° are examples of this. In summary, three different criteria and a fair number of examples of each indicate the dark areas are highlands.

7. DISCUSSION OF RESULTS

The results of Table 6 indicate characteristic slopes of the Martian dark areas of 1 - 4° and peak altitudes of many kilometers. Upper limits to the heights of Martian mountains have been sought by observations of the limb. Lowell (1906) set an upper limit, by this method, of 0.8 km; but Tombaugh (1961) has shown that 8 km is a more realistic limit. However, both these observers are describing contrast determinations assuming steep slopes, and, further, assuming that the bright areas are the elevations. Contrast determinations at the limb are much more difficult if the dark areas are highlands and the slopes shallow.

The characteristic yield and tensile strengths of ordinary solids are $S \sim 3 \times 10^9$ dynes cm^{-2}. The maximum heights that can be supported are $S/\rho g$, where ρ is the mean density of the elevation material and g is the local acceleration due to gravity. For the Earth this yields maximum elevations $\simeq$ 10 km, or slightly greater than the height of Mt. Everest and higher than the highest seamounts. On the same basis, elevations as high as about 25 km are allowed on Mars, because of the smaller value of g. The derived elevations of Table 6 are, therefore, consistent with strengths of plausible materials. These remarks are independent of the degree of isostatic compensation on Mars. Note that had we assumed the radar returns were from lowlands rather than highlands, the derived slopes would have been on occasion more than twice as steep, and the resulting load of highland (under this assumption, bright area) material would have exceeded reasonable yield and tensile strengths.

The derived slopes also do not seem unreasonable. In the absence of local erosion producing local peaks and valleys, slopes of a few degrees for mountain ranges are common on the Earth. Beneath the oceans, a typical slope for the continental rise (now covered with turbidity current sediments) is 1°, and for the continental slopes, 3-5°.

The general picture of Mars that emerges from this study — lowland basins gently sloping to highlands, some of which may be flat on top — resembles the expected appearance of the Earth were the oceans removed. If we imagine the vertical relief enhanced by a factor of $g_{\oplus}/g_{\sigma} = 2.5$, and the absence of sedimentation on the continental rises and water erosion features on the continents, the similarity is improved. In the absence of water, the old continental shields (e.g., the Canadian, Brazilian, and Rhodesian Shields) should be at a local elevation maximum (Heezen, 1966), and it is possible that the continents should slope downward toward the ocean basins from their centers. There is no reason to believe that the principal geological features of the Earth such as continents and ocean basins, rifts, ridges, and mountain ranges are critically dependent on the presence of water for their existence; water operates chiefly to reduce the prominence of these features. On Mars the basins seem to be filled with dust. Aeolian erosion should be much less efficient than erosion due to running water.

We see from Tables 4 and 5 that the two most prominent "canals" encountered in the 1965 radar swath, Deuteronilus and Ceraunius, both have slopes of several degrees and widths of a few hundred km. These slopes and dimensions are roughly comparable to those of continental terrestrial mountain ranges, if uneroded; of the centers of oceanic ridges; and of chains of seamounts. On the other hand, features with particularly shallow inclinations (Tables 4 and 6) are Nodus Laocoöntis, Nepenthes, Trivium Charontis (northern slopes), and Niliacus Lacus (western slopes). Of the areas for which slopes are available in this

study, the first three of these regions are the three for which the most striking secular changes have been reported (Antoniadi, 1930; Slipher 1962), and it seems possible that secular changes are to be attributed to drifts of dust onto and off of elevations of low slopes. Also consistent with this picture, the regions of highest elevations, Moeris Lacus, Syrtis Major, and Niliacus Lacus, correspond to the most prominent dark areas near the radar swath.

In some views of the origin of continents on the Earth, convection is invoked in the mantle, between the growing iron core and the crust (Vening Meinesz, 1962). From the dynamical oblateness of Mars and models of its interior structure, several authors have concluded it to be more nearly homogenous than is the Earth (see, e.g., Urey, 1952). The sizable amounts of surface iron on Mars suggest that iron has not largely migrated to the interior on that planet (Sagan, 1966). Finally, the negative results in the search for a Martian magnetic field by Mariner 4 (Smith, Davis, Coleman, and Jones, 1965; van Allen, Frank, Krimizis, and Hills, 1965; O'Gallagher and Simpson, 1965) also seem to imply the absence of a conducting liquid core. But if, as we have concluded in the present paper, there are continental blocks on Mars, they could not have formed by a process of mantle convection between two spherical shells, one of them the core-mantle interface.

8. CONCLUSIONS

From the quasi-specular component of the radar power reflectivity as a function of Martian longitude, and from the radar Doppler spectra also as a function of longitude, the Martian dark areas have been found to have systematically higher elevation than the adjacent bright areas. Slopes of a few degrees are deduced, and elevation differences up to 17 km are inferred. These slopes and elevations are similar to those expected for the Earth if oceans and water erosion were removed and the acceleration due to gravity decreased by a factor 2.5. Steep slopes are found for the "canals," shallow slopes for Nix Olympica and areas noted for their secular changes, and the highest elevations are deduced for the most prominent dark areas. Other consequences of these conclusions – for the seasonal and secular changes, the canals, the surface pressures, and the oblateness of Mars – will be discussed elsewhere.

The deduced slopes and altitudes are uncertain to at least 50%, and improved observations with superior signal-to-noise ratios are greatly needed. Future oppositions will move the swath of the subterrestrial point to more southerly latitudes, and we expect prominent radar returns from bright areas surrounded by dark areas, e.g., Libya, latitude +5°, longitude 275°. When range-Doppler mapping becomes feasible the thesis of the present paper can be checked by an independent method. For example, in the 1965 opposition, it would have been useful to find the range of the quasi-specular central peaks for longitudes 200-210° and 270-280°. We would expect a significant fraction of the central power to originate at positions displaced from the subterrestrial point, and corresponding to adjacent dark areas. Eventually an even more

direct test can be performed of the elevation differences derived here. A 10-km elevation difference corresponds to a radar propagation-time difference of 60 μ sec. Because of the rapid rotation of Mars and its distance, this time delay is not yet measurable, but such an experiment should be feasible in the not very distant future (Shapiro, 1966).

9. ACKNOWLEDGMENTS

We are indebted to Drs. A. Dollfus and J. H. Focas for forwarding the map prepared from Dr. Focas' 1965 visual observations of Mars; to Dr. Rolf Dyce for making preliminary Arecibo power-spectra reductions available to us in advance of publication; to Drs. Bruce Heezen and Irwin Shapiro for informative discussions on submarine geology and radar technology, respectively; and to Mrs. Elinore Green for planimetering the radar spectra.

10. REFERENCES

ANTONIADI, E.-M.

1930. La Planète Mars. Libraire Scientifique Hermann et C^{ie}, Paris, 239 pp.

DOLLFUS, A.

1961. Visual and photographic studies of planets at the Pic du Midi. In Planets and Satellites, The Solar System, vol. III, ed. by G. P. Kuiper and B. M. Middlehurst, Univ. of Chicago Press, Chicago, pp. 534-571.

1965. Private communication.

DYCE, R. B.

1965. Recent Arecibo observations of Mars and Jupiter. NBS Journ. Res., Section D, Radio Science, vol. 69D, no. 12, pp. 1628-1629. Paper 69D12-613, Session V, Radar Observation of the Planets.

1966. Private communication.

GOLDSTEIN, R. M.

1965. Mars: Radar observations. Science, vol. 150, pp. 1715-1717.

GOLDSTEIN, R. M., AND GILLMORE, W. F.

1963. Radar observations of Mars. Science, vol. 141, pp. 1171-1172.

HEEZEN, B.

1966. Private communication.

KOTELNIKOV, W. A., DUBROVNIN, W. M., DUBINSKIJ, B. A., KISLIK, M. D., KUSNEZOV, B. I., PETROV, G. M., RABOTJAGOV, A. P., RSHIGA, O. N., AND SCHACHOVSKOJ, A. M.

1963. Radiolocation of Mars in the Soviet Union. Doklady Akad. Nauk S. S. S. R., vol. 151, pp. 811-814.

LOWELL, P.

1906. Mars and Its Canals. Macmillan Publ. Co., New York.

O'GALLAGHER, J. J., AND SIMPSON, J. A.

1965. Search for trapped electrons and a magnetic moment at Mars by Mariner IV. Science, vol. 149, pp. 1233-1239.

PETTENGILL, G. H.

1965. A review of radar studies of planetary surfaces. NBS Journ. Res., Section D, Radio Science, vol. 69D, no. 12, pp. 1617-1623. Paper 69D12-609, Session V, Radar Observations of the Planets.

POLLACK, J. B., AND SAGAN, C.

1966. Radar Doppler spectroscopy of Mars. II. Subsurface structure and composition. Smithsonian Astrophys. Obs. Spec. Rep., to be published.

SAGAN, C.

1966. Mariner IV observations and the possibility of iron oxides on the Martian surface. Letter to the Editor, Icarus, vol. 5, no. 1, pp. 102-103.

SAGAN, C., AND POLLACK, J. B.

1965. Radio evidence on the structure and composition of the Martian surface. NBS Journ. Res., Section D, Radio Science, vol. 69D, no. 12, p. 1629. Paper 69D12-614, Session V, Radar Observations of the Planets.

1966. Elevation differences on Mars. Smithsonian Astrophys. Obs. Spec. Rep., in press.

SHAPIRO, I. I.

1966. Private communication.

SLIPHER, E. C.

1962. The Photographic Story of Mars. Ed. by J. S. Hall, Sky and Publ. Corp., Cambridge, Massachusetts, 168 pp.

SMITH, E. J., DAVIS, L., JR., COLEMAN, P. J., JR., AND JONES, D. E.

1965. Magnetic field measurements near Mars. Science, vol. 149, pp. 1241-1242.

TOMBAUGH, C. W.

1961. A remark in The Atmospheres of Mars and Venus, prepared by W. W. Kellogg and C. Sagan, Publ. 944, National Academy of Sciences – National Research Council, Washington, pp. 66-67.

UREY, H. C.

1952. The Planets. Yale Univ. Press, New Haven, 245 pp.

VAN ALLEN, J. A., FRANK, L. A., KRIMIZIS, S. M., AND HILLS, H. K.

1965. Absence of Martian radiation belts and implications thereof. Science, vol. 149, pp. 1228-1233.

VENING MEINESZ, F. A.

1962. Thermal convection in the earth's mantle. In Continental Drift, International Geophysics Series, vol. 3, ed. by S. K. Runcorn, Academic Press, New York, pp. 145-176.

NOTICE

This series of Special Reports was instituted under the supervision of Dr. F. L. Whipple, Director of the Astrophysical Observatory of the Smithsonian Institution, shortly after the launching of the first artificial earth satellite on October 4, 1957. Contributions come from the Staff of the Observatory.

First issued to ensure the immediate dissemination of data for satellite tracking, the reports have continued to provide a rapid distribution of catalogs of satellite observations, orbital information, and preliminary results of data analyses prior to formal publication in the appropriate journals. The Reports are also used extensively for the rapid publication of preliminary or special results in other fields of astrophysics.

The Reports are regularly distributed to all institutions participating in the U. S. space research program and to individual scientists who request them from the Publications Division, Distribution Section, Smithsonian Astrophysical Observatory, Cambridge, Massachusetts 02138.